Risk neutral pricing of weather derivatives and their applications in hedging energy generation assets.

Nicky Sonnemans - 506125

Erasmus University Rotterdam

Supervisors
dr. Dick van Dijk

02 April 2024

Abstract

This research delves into the potential of weather derivatives, specifically temperature derivatives, in hedging energy assets across Europe. With increasing climate variability, there's a heightened demand for effective risk management tools. The study decomposes temperature data from 18 European cities between 2000-2023 and simulates temperature derivatives, it utilizes energy generation data between 2018-2023. The findings reveal that these derivatives can significantly reduce the variance of energy portfolios, especially in Southern European countries. While the decomposition model effectively captures temperature dynamics, residuals still exhibit slight non-normality. The research also unveils differences in hedging preferences among energy types. The study's methodologies and data are open-sourced for further exploration.

Contents

1 Introduction

Weather derivatives are financial instruments designed to help manage risk associated with adverse weather conditions. They enable parties to hedge or speculate on the financial impact of future weather events, such as temperature, precipitation, or wind CME Group [2021]. Temperature derivatives are of particular interest to businesses in the energy and agriculture sectors, as well as other industries that are sensitive to temperature fluctuations. For example, energy companies may use these to hedge against the risk of unusually warm or cold seasons, which can significantly impact their revenues. Similarly, agricultural producers may use these instruments to protect against crop losses due to extreme temperature events.

Over the past few years, the demand for weather derivatives has increased substantially, reflecting the growing need for effective risk management tools in the face of increasing climate variability and extreme weather events. The increased demand for weather derivatives has led to a greater need for accurate pricing models and methods for hedging energy assets. This has been facilitated by the improved availability of weather data from sources such as the European Centre for Medium-Range Weather Forecasts (ECMWF), and the National Oceanic and Atmospheric Administration (NOAA).These data sources provide a wealth of information for developing sophisticated risk-neutral pricing models for weather derivatives, which can be tailored to specific assets, industries and regions.

This thesis focuses on managing risks associated with energy assets using weather derivatives. In this research, continuous-time autoregressive moving-average (CARMA) models are utilized for the simulation of future weather conditions (temperature) in different cities across Europe. Using these simulations, daily price series of temperature derivatives can be constructed. For simplicity, we assume in this thesis that we can buy an w_i amount of temperature derivatives at the beginning of each month which must be held throughout the entire month, where $i = 1, 2, .., 11, 12$. Using the *full sample*, we construct a portfolio of the combined revenue of each energy generation type and the weather derivatives for different countries in each month.

The usage of CARMA models to model weather parameters and eventually price weather derivatives is well-documented, but integrating these derivatives with electricity asset revenues for portfolio construction is less explored. Our work contributes to the literature by analyzing the effectiveness of modern portfolio theory in this context, using a full sample for weight construction and evaluation. This approach is due to the limited sample size in each portfolio, with only around 150 $(5 * 30)$ observations per portfolio from five years of generation data as the portfolios are constructed on a monthly basis.

As the temperature is not only a predominant factor in energy usage, e.g. heating or AC, but also energy generation through solar, its influences on prices are quite large. However, it's not clear to what extent the weather derivatives can have impact on different energy portfolios. Given this, the following research questions (RQ) are proposed:

1. How can temperature be effectively decomposed for use in weather derivative pricing models?
2. How effective are temperature derivatives at hedging energy portfolios?
3. How do different energy asset types (e.g., wind farms, solar power plants, and conventional power

plants) influence the effectiveness, or use, of a temperature derivative for hedging purposes?

Firstly, given the extensive research done on modeling weather parameters, a lot of methodology has been developed on decomposing the seasonality of temperature and wind. However, due to the lack of data, this methodology has often been tested on just a single geography. With the first RQ, we provide statistics and results for multiple locations across Europe.

For the second and third RQ, we draw on modern portfolio theory. We find the global minimum variance portfolios for multiple energy generation types, compute the reduction in variances, and compare their results.

The main findings of this thesis are as follows. While the methodology developed to capture and decompose the dynamics of temperature is extensive, it doesn't fully convert the residuals of temperature in white noise. There is still a slight auto correlation, accompanied by some excess kurtosis and (positive) skew in the residuals. However, using the modeled derivatives, we observed a significant reduction in the variance of the energy portfolios, ranging between 1% and 20%. In addition to this, there are some visible differences in how the weights are composed for the temperature derivatives for different energy generation types. For wind, the weights indicated that protection against colder winters was deemed necessary, while for other generation types, the preference for protection against hotter winters was given. This finding, aligns with the operational characteristics of wind energy, which is often higher in colder conditions due to increased wind speeds. As a result, there is a necessity for hedging against unusually cold winters which might lead to excess supply and lower prices. The author's key contribution in this thesis is the development and open-sourcing of the code for the fundamental aspects of pricing weather derivatives. This code not only covers the basics of derivative pricing but also facilitates easier access to the necessary data, something which as of the author's knowledge has not yet been done.

The rest of the thesis is organized as follows. Section 2 presents a background on electricity markets and weather derivatives, Section 3 presents the data utilized in this thesis. In Section 4 we present models for temperature decomposition, and the continuous-time simulation of weather derivatives. Next, in section 5 we present the results. Finally, section 6 concludes the thesis.

2 Background

In this chapter, the background for this thesis is provided. Given the use of weather derivatives to hedge energy assets, it's helpful for readers to grasp the workings of the electricity grid and the dynamics of electricity markets.

The first section sheds light on the European electricity grid. This is followed by an explanation of how financial electricity markets are orchestrated in Europe. The subsequent part gives an overview of the market in weather derivatives. To conclude, a review of relevant literature on weather derivatives and their applications is presented.

2.1 Electricity Grid

The main grid actors on the European electricity grid are the Transmission System Operators (TSO), the Balance Responsible Parties (BRP), and the Balance Service Providers (BSP). The TSO is responsible for the reliable transmission of power from generation plants to regional or local electricity Distribution System Operators (DSO) using the high-voltage electricity grid. The TSO holds a natural monopoly and is tasked with maintaining the electricity grid. The BRP is an entity that can and may handle the balancing responsibility for production and consumption units and/or trades actual electricity units. The BSPs are market participants that provide balancing energy and balancing capacity to the TSO. Examples of these entities include TenneT as a TSO; Enexis as a DSO; Eneco Energy Trade as a BRP; and Giga Storage as a BSP (capacity trader). For additional examples, refer to the EIC approved codes. An overview of the organization of European electricity balancing markets is presented in Figure 1 (Tolstrup et al. [2020]).

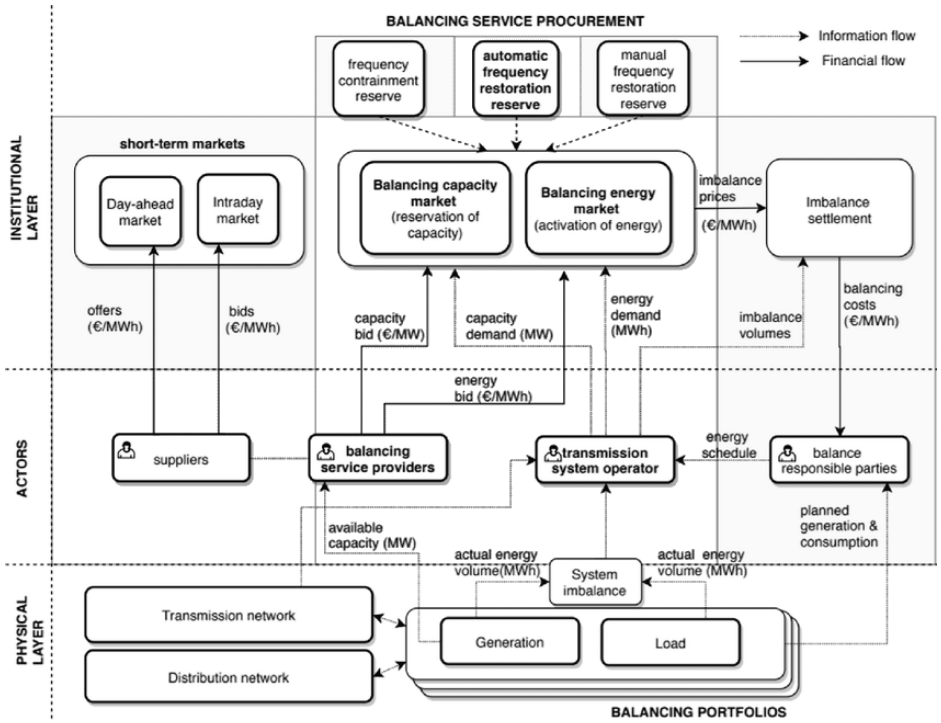

Figure 1: Overview of the organization of European electricity balancing markets. The focus of this thesis is on the short-term markets, in particular the Day-ahead market. Adapted from Tolstrup et al. [2020].

Every day, various grid actors engage in interactions to ensure a continuous match between electricity demand and supply. Failure to achieve this balance can lead to frequency deviations, leading to system malfunctions within the grid. The key grid actors involved in this process are the Transmission System Operator (TSO), the Balance Responsible Party (BRP) and the Balance Service Provder (BSP). The TSO plays a crucial role in securing bids for the balancing market to ensure an adequate supply of balancing power. The BRP serves as the link between electricity consumption and generation. The BRP also bears responsibility for managing imbalances resulting from deviations between this link. At the end of each day, any discrepancies between actual and forecasted consumption are settled through an imbalance system. The Balancing Services Provider (BRP) provides short-term balancing services, also known as ancillary services, to the electricity grid. They play a critical role in balancing out short-term grid deviations to ensure grid security.

Electric power generation is mainly done by thermal power plants, using fossil fuels or nuclear fission to convert thermal energy to electric energy. More recently, renewable energy is playing a more prominent role in the supply of electricity, owing to the declining costs of these energy sources and the implementation of supportive policies. The recent surge in growth can be attributed to onshore wind farms and solar photovoltaic farms, with an anticipated increase in offshore wind electricity generation in the coming years.

Figure 2 and Table 1 highlight the total energy mix for the countries discussed in this thesis. A notable trend from these references is the rapid growth of renewable energy, solar photovoltaic in particular. Many countries, with the exception of the Nordics, France, and Switzerland, predominantly depend on fossil fuels, with gas being a major contributor. France, however, is distinguished by its significant nuclear-installed capacity. On another note, Norway, despite being one of the world's leading natural gas exporters, primarily relies on hydro for its energy production. It's important to highlight that large renewable capacities don't always equate to their full contribution to the energy generation mix, given the weather-dependent nature of renewable energy.

	Austria	Belgium	Switzerland	Germany	Denmark	Spain	France	Italy	Netherlands	Norway	Portugal	Sweden
	AT	BE	CH	DE	DK	ES	FR	IT	NL	NO	PT	SE
biomass	0.48	0.71	-	8.47	1.75	0.71	1.34	1.53	0.42	-	0.68	-
fossil (brown coal lignite)	-	-	-	17.69	-	-	-	-	-	-	-	-
fossil (coal derived gas)	-	-	-	1.26	-	-	-	2.07	-	-	-	-
fossil (gas)	4.21	6.92	-	31.81	1.57	29.90	12.89	44.22	18.35	0.46	4.52	-
fossil (hard coal)	-	-	-	18.13	3.02	3.22	1.82	5.58	4.01	-	-	-
fossil (oil)	0.12	0.46	-	4.08	0.96	0.67	2.57	1.54	-	-	-	-
geothermal	-	-	-	0.06	-	-	-	0.87	-	-	-	-
hydro (pumped storage)	3.36	1.31	6.70	10.03	-	3.42	5.05	7.26	-	1.06	2.83	-
hydro (run of river)	5.90	0.19	0.60	3.72	-	1.16	11.70	10.55	0.04	6.70	2.86	-
hydro (water reservoir)	2.77	-	5.59	1.43	-	15.77	8.79	4.44	-	26.70	1.52	16.30
nuclear	-	5.94	2.97	4.06	-	7.12	61.37	-	0.49	-	-	6.90
other	0.84	0.02	-	1.71	-	0.12	1.14	0.85	-	0.03	0.03	9.00
other (renewable)	-	-	-	0.38	0.14	0.28	-	-	-	0.10	-	-
solar	3.26	6.48	-	63.07	2.32	18.52	14.64	5.43	22.59	-	1.03	-
waste	0.10	0.38	-	1.91	0.38	0.55	0.93	0.12	0.79	0.09	-	-
wind (offshore)	-	2.25	-	8.13	2.31	-	0.49	0.03	3.22	-	0.02	-
wind (onshore)	3.57	2.99	-	57.59	4.71	29.32	20.84	11.20	6.19	5.13	5.33	14.70
Total	24.61	27.65	15.86	233.53	17.16	110.76	143.57	95.69	56.10	40.27	18.82	46.90

Table 1: Table of the installed capacity in GW of different energy sources for the countries of interest in this thesis. The installed capacity is measured on the 1st of January 2022.

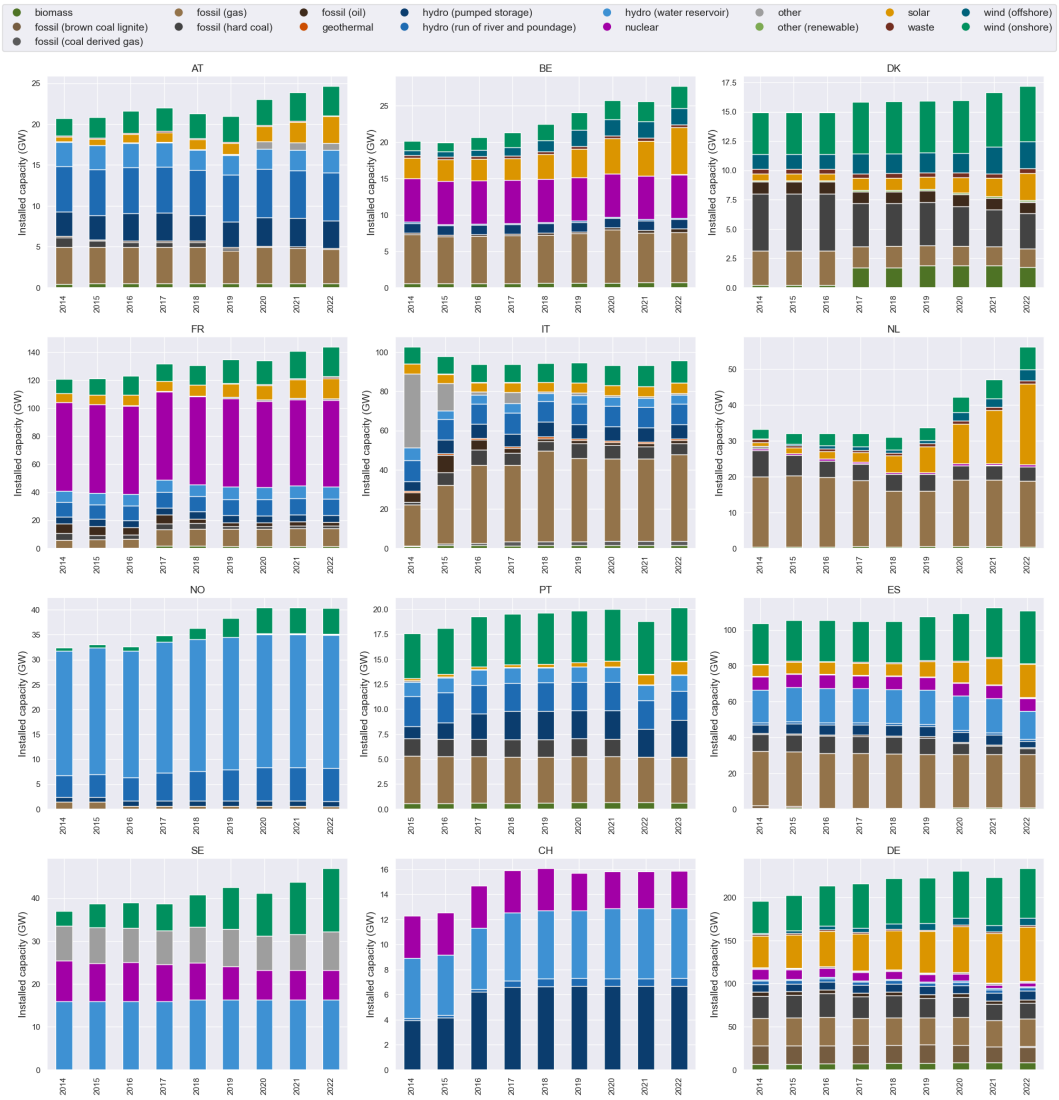

Figure 2: Historical series of the installed capacity in GW of different energy sources for the countries of interest in this thesis.

2.2 Electricity Markets

Since the market liberalization that started in the early 1990s, the introduction of competitive markets in the electricity grid has reshaped the landscape of monopolistic and government-controlled energy sectors. Currently, the economic law of supply and demand determines the price in marketplaces where electricity can be traded in either spot or forward contracts.

The European electricity market follows a sequential model, where energy is procured on various time horizons before the actual energy exchange event. This process can be categorized into year-ahead, month-ahead, week-ahead, day-ahead, and intraday markets. For the purpose of this research, the focus primarily lies on the day-ahead markets.

In each European country, the TSO designates ones (or multiple) parties as the Nominated Electricity Market Operator (NEMO). These are granted the authority to operate the day-ahead and intraday

markets. For example, within the Netherlands, EPEX spot and Nordpool have been designated.

As discussed, the trading of electricity, both physically and financially, can start many years ahead in forward markets. Long-term energy trading is a strategy adopted to mitigate the market risk associated with fluctuating energy prices and allow hedging for producers and consumers. These markets continue until one day before delivery (of the actual energy exchange). Afterwards, the Day-Ahead market runs until 12:00 AM (in most countries), in which energy players must submit their bids for all hours in the subsequent day. After this bidding process, the intraday market opens in which energy players can freely trade electricity until delivery. During delivery, the balancing market opens to ensure a continuous match between demand and supply. This process is schematically displayed in Figure 3.

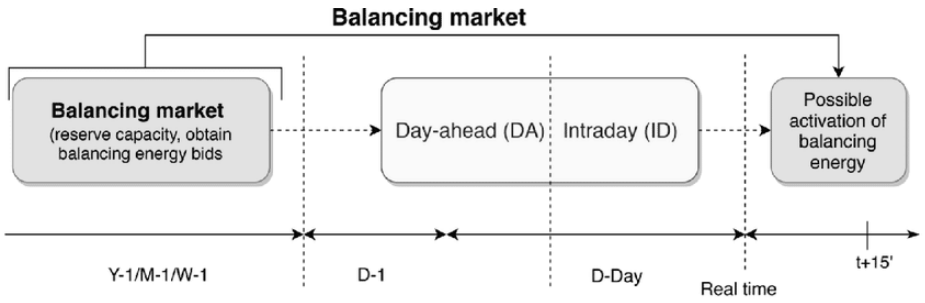

Figure 3: Overview of the temporal sequence of European electricity balancing and spot markets. The focus of this thesis is on the short-term markets, in particular the Day-ahead market. Adapted from Tolstrup et al. [2020].

To tackle the complex physical reality of the grid when trading electrical energy, zonal pricing has been developed. Zonal pricing means that wholesale electricity prices can differ between bidding zones in Europe. From the market perspective, the network within a bidding zone is considered to be a copper plate - physical capacity is treated as infinite. The different bidding zones within Europe can be found in Figure 4, while they mostly follow the borders of countries, some countries are subdivided into additional bidding zones.

These bidding zones play a role in this thesis due to several reasons. Firstly, the weather patterns and their financial implications on energy assets can vary significantly across these zones. This could directly impact the pricing and effectiveness of the weather derivatives. Secondly, as this thesis delves into the hedging of energy assets using weather derivatives, understanding the zonal distinctions helps in tailoring hedging strategies to specific regions.

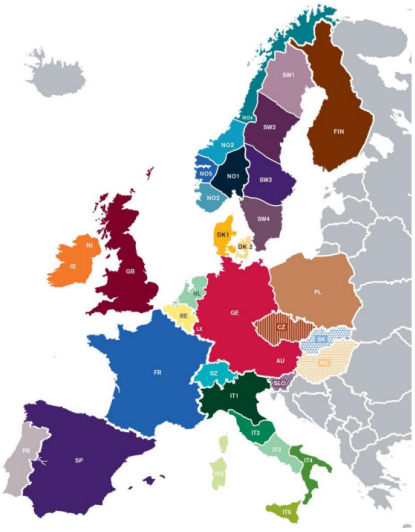

Figure 4: Overview of the different bidding zones in the European electricity grid. Each colored area is a different bidding zone. Sourced from OFGEM.

2.2.1 Day-Ahead Market

Closer to delivery, electricity is traded in the short-term markets.
These are composed of the day-ahead market, intraday markets,
and the real-time balancing market. The day-ahead market, is an
auction typically held between 36 to 12 hours before the actual energy delivery. Market participants that have not yet committed their electricity supply or demand through bilateral contracts submit their bids and offers to the NEMO. At the clearing time, at 12:00 the day before delivery, the NEMO combines all bids and offers according to a public couple merit order algorithm. This algorithm matches demand and supply within the whole operating zone of the NEMO, also accounting for cross-border capacity and different bidding zones.

The consolidation of bids and offers follow a merit order system, where the highest marginal accepted bid determines the price for all other bids. As coupling between bidding zones is executed implicitly, any price disparities between different bidding zones can only arise if the cross-border capacity is fully utilized. Additionally, the algorithm couples different NEMOs, ensuring that prices on all exchanges are aligned.

Prices on the day-ahead electricity market are subject to influences, such as commodity prices, weather conditions, infrastructure limitations, and unusual occurrences. Given the coupling of the entire European electricity market, events occurring in one region can have ripple effects on the other side of the continent. Weather-related incidents, such as Germany experiencing low river levels leading to challenging coal shipments to the Rhine region, can significantly affect electricity market dynamics. Similarly, extreme storms may require wind turbines to be curtailed, subsequently leading to higher electricity prices. Unusual occurrences, like an influx of extreme jellyfish, can have unexpected consequences, such as clogging water cooler units in nuclear plants. These occurrences add to the complexity of managing electricity market operations and supply.

2.2.2 Intraday and the imbalance settlement market

After the day-ahead power auction, producers and consumers have the possibility to continuously adjust their positions through intraday markets. This flexibility ensures the BRPs can further correctly match supply and demand based on new information, and in doing so, limit their exposure to the imbalance market. IIntraday trading remains open until a specific moment known as the intraday gate closure time (GCT), after which the final production schedule is determined for all market participants. Once the GCT is reached, only the TSO can act to adjust deviations between supply and demand using the balancing mechanism. This balancing mechanism operates through two distinct balancing markets: the balancing market for capacity and the balancing market for energy.

The balancing market for capacity occurs between one year and one day before real-time. During this period, generators or demand providers are contracted to be available to deliver balancing capacity in real-time. The second market, the balancing market for energy, allows participating generators or demand providers to indicate the price at which they are willing to increase or decrease their energy injection or withdrawal in real-time

In real-time, the TSO activates the least-cost resources with the necessary technical capabilities to rectify imbalances between electricity generation and consumption.

2.2.3 Power Purchase Agreements

In practice, a significant number of electricity generators do not actively participate in the electricity markets; instead, they directly sell their electricity through a BRP. This arrangement involves the signing of a Power Purchase Agreement (PPA) between the electricity generator and the BRP. PPAs are contracts that outline the terms of electricity purchase and can be structured based on either a fixed price or be linked to market prices. These agreements serve as a means of securing a steady income for electricity generators and providing stability for the BRP in meeting their customers' electricity demands.

PPAs can vary in duration, from short-term contracts covering a few years to long-term agreements spanning several decades. Prices may be flat, escalate over time, or be negotiated in any other way. The most common PPA pricing structures can be found in Figure 5.

Within the fixed price nominal PPA, the buyer locks in a fixed electricity price for the duration of the PPA contract. This fixed price is often based upon the price of a power future contract. In this contract, the buyer completely bears the electricity price risk. One may also have a fixed price nominal PPA with an escalation, to capture inflationary effects. Additional options include a discount to market, a collar structure, or a hybrid structure. Many of the different types of PPA structures can be summarised using the following equation:

$$f(P_t; P_f, \phi, \lambda, \delta, \mathrm{C}, \mathrm{F}) = \begin{cases} \mathrm{C}, & \text{if } f(P_t; P_f, \phi, \lambda, \delta, \mathrm{C}, \mathrm{F}) < \mathrm{C}, \\ \mathrm{F}, & \text{if } f(P_t; P_f, \phi, \lambda, \delta, \mathrm{C}, \mathrm{F}) > \mathrm{F} \\ \lambda(P_f + \phi) + (1-\lambda)(1-\delta)P_t, & \text{otherwise.} \end{cases} \tag{1}$$

Where P_t is the day-ahead (hourly) price of electricity at time t, P_f is the fixed price of electricity. For simplicity, this thesis will assume the fixed price of electricity to be the median electricity price of the quarter of time t (Q1, Q2, Q3, Q4). The weight of the fixed price component is represented by λ, and the premium on the fixed price can be set through ϕ. The collar is represented by C (cap) and F (floor). Finally, the discount to market is controlled through δ.

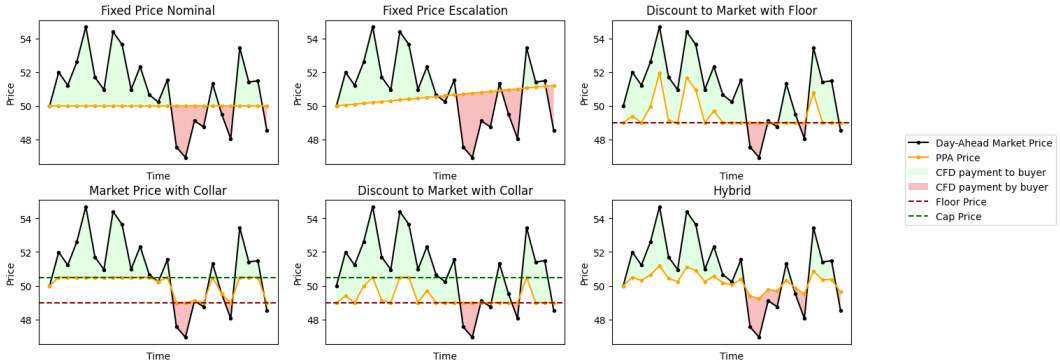

Figure 5: Overview of different PPA pricing structures from Equation 1. The data is fictional.

Within the context of the thesis, it is helpful to understand the nuances of different PPA structures. These structures influence the revenue of energy assets and therefore shape the strategies for using weather derivatives as hedging tools.

2.3 Weather Derivatives

Weather derivatives are financial instruments designed to help manage risk associated with adverse weather conditions. They enable parties to hedge or speculate on the financial impact of future weather events, such as temperature, precipitation, or wind. Temperature derivatives are of particular interest to businesses in the energy and agriculture sectors, as well as other industries that are sensitive to temperature fluctuations. For example, energy companies may use these to hedge against the risk of unusually warm or cold seasons, which can significantly impact their revenues. Similarly, agricultural producers may use these instruments to protect against crop losses due to extreme temperature events.

The main exchange where weather derivatives are traded is the Chicago Mercantile Exchange (CME). More recently, EPEX Spot, a power exchange, together with Speedwell Climate cooperatively launched new weather-based power indices for different European countries. These are used for OTC pricing and are not traded on an exchange but rather used by reinsurance parties to help create standardized contracts. In addition to this, Nasdaq Commodities provide tradable wind power futures by utilizing NAREX WIDE as the underlying index to settle on the relative German wind power utilization. The NAREX WIDE is a specific synthetic index that calculates the German wind power production, it's a bottom-up model calculated by StormGeo, essentially summing unique power forecasts for each wind asset. The index is based on data from the ECMWF weather forecasting model.

Except for weather futures traded on the CME, which use measured temperatures from a specified weather station in the vicinity for settlement prices, using weather data for pricing from ECMWF either directly or indirectly is the industry standard.

2.3.1 Temperature Futures

This thesis will focus specifically on how the weather futures on the CME are structured. Therefore, we will explain how weather is traded on the CME exchange. As discussed, the weather products quantify weather in terms of how much the temperature deviates from the monthly or seasonal average in a particular city, allow market participants to trade the weather much like any other commodity index.

The value of a future is determined by the value of the underlying weather index, measured in Heating Degree Days (HDD) or Cooling Degree Days (CDD) - the total number of degrees that the average outside air temperature falls or rises below or above the base temperature of 18°C. The European summer cooling month contracts are based on a Cumulative Average Temperature (CAT). Each monthly CAT index is simply the accumulation of daily average temperatures recorded in degrees Celsius over a calendar month. The HDD is especially useful in winter, to measure the demand for heating. Conversely, the CAT/CDD is useful in the summer, to measure the demand for air conditioning.

For example, we take the HDD and CDD contract. If on a certain day the average temperature was 20°C, the value of the HDD would be 2, and the value of the CDD would be 0. When evaluating a monthly contract, where on each day the measured average temperature was as in our example, an average temperature of 20°C Accordingly, the cumulative monthly HDD would equal 60 (2 HDDs x 30 days). The value at settlement would be determined by multiplying the cumulative HDD or CDD by the contract's tick size, which in the CME's case is $20. Therefore the final value would equal $1200.

The CME has its weather futures and options listed in strip contracts that span a couple of months. The HDD contract consists of a nov-mar (November to March) strip, and a dec-feb (December to February) strip. The CDD contract consists of a may-sep (May to September) strip and a jul-aug (July to August) strip. Within Europe the CDD is replaced by the CAT index. For completeness, an overview of the weather futures traded are given in Figure 6. For simplicity, this thesis will use fictionalized monthly futures that only span single months.

HEATING (HDD) FUTURES AND OPTIONS

U.S.	CITY CODE	NOV-MAR STRIP	DEC-FEB STRIP
Atlanta	H1	H1X	H1Z
Boston	HW	HWX	HWZ
Burbank	LP	LPX	LPZ
Chicago	H2	H2X	H2Z
Cincinnati	H3	H3X	H3Z
Houston	HR	HRX	HRZ
New York	H4	H4X	H4Z
Dallas	H5	H5X	H5Z
Las Vegas	H0	H0X	H0Z
Minneapolis	HQ	HQX	HQZ
Sacramento	HS	HSX	HSZ
Philadelphia	H6	H6X	H6Z
Portland	H7	H7X	H7Z
EUROPE			
Essen	D4	D4X	D4Z
London	D0	D0X	D0Z
Amsterdam	D2	D2X	D2Z
Paris	D1	D1X	D1Z

COOLING (CDD) FUTURES AND OPTIONS

U.S.	CITY CODE	MAY-SEP STRIP	JUL-AUG STRIP
Atlanta	K1	K1K	K1N
Boston	KW	KWK	KWN
Burbank	KP	KPK	KPN
Chicago	K2	K2K	K2N
Cincinnati	K3	K3K	K3N
Houston	KR	KRK	KRN
New York	K4	K4K	K4N
Dallas	K5	K5K	K5N
Las Vegas	K0	K0K	K0N
Minneapolis	KQ	KQK	KQN
Sacramento	KS	KSK	KSN
Philadelphia	K6	K6K	K6N
Portland	K7	K7K	K7N

CUMULATIVE AVERAGE TEMPERATURE (CAT) FUTURES AND OPTIONS

EUROPE	CITY CODE	MAY-SEP STRIP	JUL-AUG STRIP
Essen	G4	G4K	G4N
London	G0	G0K	G0N
Amsterdam	G2	G2K	G2N
Paris	G1	G1K	G1N

PACIFIC RIM		NOV-MAR STRIP	DEC-FEB STRIP
Tokyo	G6	G6X	G6Z
		MAY-SEP STRIP	**JUL-AUG STRIP**
		G6K	G6N

Figure 6: Overview of the weather futures and options codes traded on the CME.

2.4 Literature Review

We review some of the relevant literature on stochastic modeling of weather variables, and their financial applications. We will first review studies concerning stochastic modeling of temperature. Afterward, we will review studies that hedge energy portfolios using these derivatives.

Tol [1996] proposed to use a GARCH (Generalized Autoregressive Conditional Heteroskedasticity) model to evaluate daily temperature observations, arguing that the predictability of meteorological variables shows regular variations. He employed this model using 30 years of daily temperature data from De Bilt, The Netherlands. Using the same dataset, Franses et al. [2001] used the QGARCH model that enables asymmetry in how innovations impact conditional variance.

Building upon this, Dornier and Querel [2000] suggested a general Ornstein-Uhlenbeck dynamics model with time-varying variance for temperature time series in Chicago, although their empirical examination considered only a constant variance specification. Using a similar model, Alaton et al. [2002] applied it to data gathered from Bromma, Sweden, introducing the time-dependent variance as a constant variance over each different month.

The usage of CARMA models to model weather parameters and eventually price weather derivatives is well-documented, e.g. Cabrera [2010] used Ornstein-Uhlenbeck models driven by a fractional Brownian motion, Brownian motion or a Lévy process. She used this to transform non-tradable risk factors into tradable financial assets. In addition to this, Benth et al. [2011] and Benth and Benth [2012] particularly spearheaded the application of so-called CARMA models for weather derivatives. They proposed the continuous-time autoregressive model for temperature dynamics with volatility being the product of a seasonal function and a stochastic process, the same approach used in this thesis. By formalizing the models in higher dimensions, using CAR(p) processes, they were able to analytically determine future prices of Cooling Degree Days (CDD), Heating Degree Days (HDD), and Cumulative Average Temperature (CAT) in Benth and Benth [2012].

Owing to the heightened penetration of wind power, there has been a surge in literature investigating indices that enable the securitization of wind as well. Benth et al. [2021] employed continuous-time autoregressive models to model the wind power utilization rate at different German wind sites. After securitization, resulting in wind power futures; they compute risk premiums and discuss hedging strategies. Härdle et al. [2021] used actual electricity obtained from the TSO to fit a CARMA model and securitize the wind risk.

This thesis mainly builds upon the theoretical framework as laid out in Benth and Benth [2012], while focusing specifically on integrating these derivatives with electricity asset revenues for portfolio construction.

3 Data

This section discusses the data utilized in this thesis. Firstly, historical weather is obtained through open-meteo, which sources their weather data from the *European Centre for Medium-Range Weather Forecasts* (ECMWF). The historical weather covers the period from January 1, 2000 to June 1, 2023 on a daily sampling frequency.

In addition to this, all data pertaining to electricity is obtained from ENTSO-E. This data includes the day-ahead electricity prices, the yearly energy-mix installed capacities, actual generation per energy source and the actual generation per energy generation unit. The yearly energy-mix capacity covers 2014 to 2022. The day-ahead prices and generation data covers January 1, 2018 to June 1, 2023 on a hourly sampling frequency.

As discussed in Section 2, not all bidding zones are considered in Europe. The thesis investigates data from Austria (AT), Belgium (BE), Germany (DE), Denmark (DK), Spain (ES), France (FR), Italy (IT), the Netherlands (NL), and Portugal (PT). Weather data is requested for two major cities in each country, e.g. Copenhagen and Aarhus for Denmark, Amsterdam and Rotterdam for the Netherlands, etc.

The following table presents an overview of the different data sources used:

Data	Description	Retrieval Method	Source
	Weather		
Reanalysis: ERA5	Global reach with spatial resolution of 0.25° (approximately 25km). Hourly temporal resolution from 1959 to present.	open-meteo	ECMWF
Reanalysis: ERA5-Land	Global reach with spatial resolution of 0.1° (approximately 11km). Hourly temporal resolution from 2000 to present.	open-meteo	ECMWF
	Electricity		
Unit Generation	Hourly generation for solar, wind and other generation assets as reported to the TSO. Data is from 2018-01-01 until 2023-01-01.	entsoe-py	ENTSO-E
Generation	Hourly generation per production type as reported/calculated to the TSO. Data is from 2018-01-01 until 2023-01-01.	entsoe-py	ENTSO-E
Capacity	Yearly Capacity per production type. Data is from 2018-01-01 until 2023-01-01.	entsoe-py	ENTSO-E
Day-Ahead Prices	Hourly day-ahead electricity prices from 2018-01-01 until 2023-01-01.	entsoe-py	ENTSO-E

Table 2: Overview of data sources

The general characteristics describing the different data are shown in Table 3. Upon examining the day-ahead price data, it becomes apparent that Denmark registers the lowest average day-ahead electricity price (78.86 EUR). This is primarily attributed to its extensive wind generation mix combined with its relatively low energy consumption. However, the minimum of Denmark is not as low as in some other European countries. This can be largely attributed to Denmark's relative isolation from the broader European grid, which is otherwise tightly interconnected, leading to more synchronized price levels across the continent.

Other noteworthy features are the possibility of negative electricity prices, large outliers, and a standard deviation exceeding the mean. These features arise from the hourly variability of electricity prices, which are influenced by factors like changing weather conditions, (unplanned) outages, and fluctuating demand or supply within each hour.

Transitioning to the temperature data, a clear distinction emerges: Spain represents the warmest region, while Denmark is the coldest. The temperature gradient, which follows the North-South direction, is further supported by the moderate climates seen in other countries, as reflected in the provided statistics.

		Austria	Belgium	Germany	Denmark	Spain	France	Italy	Netherlands	Portugal
Day-Ahead Price	Count	40803	47377	47473	60298	47377	47378	82140	47379	47377
	Mean	108.24	96.34	90.19	78.86	83.89	102.32	161.36	95.14	84.14
	Std	114.27	103.33	102.80	92.33	66.71	115.32	271.13	100.70	66.60
	Min	-81.59	-500	-129.96	-129.96	0	-75.82	0	-400	0
	25%	37.39	36.64	34.46	32.47	42	36.49	48.56	37.40	42.08
	50%	57.96	54.26	50	47.05	58.39	54.20	70.53	53	58.51
	75%	145.08	115.90	102.67	86	108.52	126.80	149.80	113.78	109.19
	Max	919.64	871	871	871	700	2987.78	1750	871	651
Generation (Fossil Gas)	Count	47473	47418	235920	41663	23117	47440	205038	47473	23137
	Mean	1070.89	2449.69	3478.52	241.66	7024.93	4048.02	4848.41	4934.25	1636.19
	Std	897.70	1091.15	3234.26	168.51	3010.68	2416.44	5375.81	2411.53	957.87
	Min	0	436	0	0	0	300	0	0	102
	25%	289.25	1517	582	110	4642	2281	763	2740.25	830
	50%	924	2280	2726.25	193	6330	3713	2064	4868.50	1553
	75%	1716.75	3211	5652.75	340	8962	5778.25	8047	6909.50	2388
	Max	3926	5760	19779.75	895	17922	13816	50901	11443.50	4044
Temperature	Count	17106	17106	17106	17106	17106	17106	17106	17106	17106
	Mean	10.25	11.04	10.01	8.91	15.63	13.83	14.45	10.72	16.14
	Std	8.07	6.23	7.31	6.48	6.97	6.98	7.43	5.95	4.90
	Min	-15.80	-8.05	-17.15	-11.70	-2.40	-5.35	-6.95	-8.50	3
	25%	3.80	6.35	4.45	4.05	10.10	8.55	8.55	6.30	12.25
	50%	10.50	11.20	10.05	8.85	15	13.50	14.25	10.75	15.75
	75%	16.85	15.95	15.90	14.35	21.70	19	20.60	15.50	20.05
	Max	31.30	29.45	29.85	25.25	32.55	32.45	30.90	29.05	33.25

Table 3: General characteristics of the day-ahead prices, generation (using fossil gas), and temperatures per country. Notice that the count in Denmark of day-ahead prices is higher due to multiple bidding zones. Additionally, temperature is on daily frequency and contains aggregate statistics of two cities, whereas generation and prices are on hourly frequency.

3.1 Preliminary Analysis

As previously mentioned, the historical weather data is obtained for two major cities in Austria, Belgium, Germany, Denmark, Spain, France, Italy, the Netherlands, and Portugal. An analysis of the temperature within Denmark and France, to give the reader insight, is presented in Figure 7.

The first thing to note is that bimodal distributions can be imputed from the figure. This can be largely attributed to the summer and winter seasons. Additionally, significant large autocorrelation is present in the temperature; which are persistent over a longer period of time. These can to a large extent be attributed by the seasonality in the temperature. This indicates that constructing a model that captures both seasonality and the auto regressive nature of temperature might be sufficient in modelling the temperature.

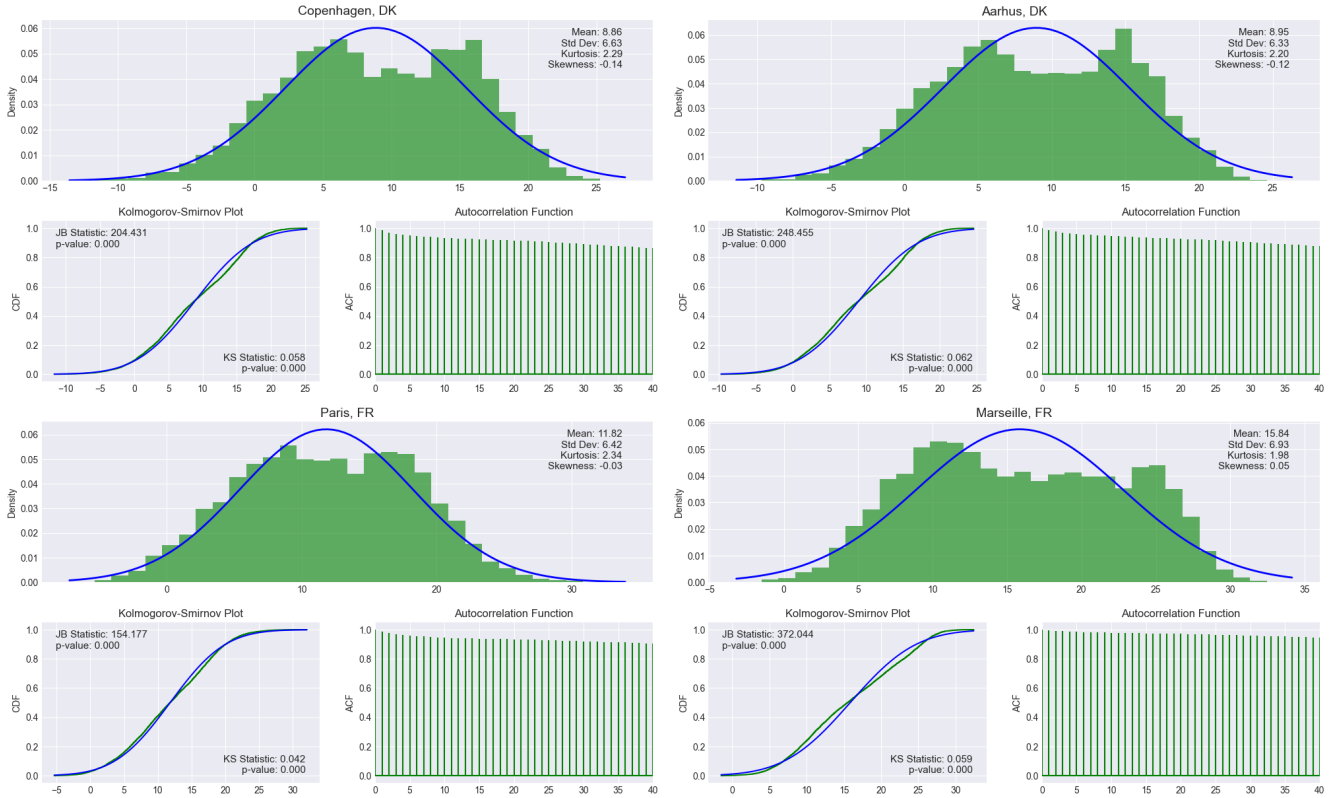

Figure 7: General analysis of temperature dynamics for a subselection of the total data. The temperature is measured 2 meters above ground and covers the period from January 1, 2000 to June 1, 2023.

4 Methodology

This section introduces the mathematics needed to model and simulate the required weather parameters, and consequently price their derivatives. Additionally, we discuss how to manage risk exposure using these derivatives.

4.1 Continuous-time autoregressive models

We introduce the continuous-time design of the ARMA models. The *continuous-time autoregressive moving-average* (CARMA) has been developed by Doob [1944] and extended to financial applications by Brockwell [2001]. We follow the methodology of Benth and Benth [2012] who used the CARMA for modeling weather parameters.

4.1.1 CARMA

Let $\mathcal{B}$ be a Brownian motion which is defined on a *complete filtered probability space* $(\Omega, \mathcal{F}, \{\mathcal{F}\}_{t\geq 0}, P)$. Additionally, we introduce a stochastic process $\mathbf{X}(t)$ defined in $\mathbf{R}^p$ for $p \geq 1$ as the solution of the stochastic differential equation (SDE):

$$\mathbf{X}(t) = A\mathbf{X}(t)dt + \mathbf{e}_p\sigma(t)d\mathcal{B}(t) \tag{2}$$

where $\mathbf{e}_p$ the pth Euclidean unit vector. The $(p \times p)$ matrix A is defined as:

$$A = \begin{bmatrix} 0 & 1 & 0 & \cdots & 0 \\ 0 & 0 & 1 & \cdots & 0 \\ \vdots & \vdots & \vdots & \vdots & \vdots \\ 0 & 0 & 0 & \cdots & 1 \\ -a_p & -a_{p-1} & -a_{p_2} & \cdots & -a_1 \end{bmatrix}. \tag{3}$$

The constants $a_k, k = 1, ..., p$ are assumed to be *non-negative* ($\alpha_p > 0$). In order to model and account for a seasonal volatility pattern, we consider a bounded and continuous function for $\sigma(t)$ that is strictly bounded away from zero.

The solution of Equation 2 starting at time $t \geq 0$ is given by the stochastic process $\mathbf{X}(s), s \geq t$ below, the full derivation can be found in Benth and Benth [2012]:

$$\mathbf{X}(s) = \exp(A(s-t))\mathbf{X}(t) + \int_t^s \exp(A(s-u))\mathbf{e}_p\sigma(u)d\mathcal{B}(u). \tag{4}$$

For $0 \leq q < p$, define the vector $b \in \mathbf{R}^p$ with coefficients $b_j, j = 0, 1, ..., p-1$ satisfying $b_q = 1$ and $b_j = 0$ for $q < j < p$. We can now define the CARMA(p,q) process as:

$$Y(t) = b'\mathbf{X}(t) \tag{5}$$

The CAR(p) process, which is the standard workhorse of modeling weather parameters, is a special case of the CARMA(p,q) process when $q = 0$ and therefore $b = \mathbf{e}_1$. The process $Y(t)$ needs to be stationary, which happens when the eigenvalues of the matrix A have a negative real part.

4.1.2 Simulation

As the goal of this thesis is to price weather derivatives where no analytical formula exists, it becomes necessary to simulate the weather dynamics and thus a CARMA(p,q) process. This requires *Monte Carlo* (MC) simulations of the future weather conditions. This section will discuss recursive schemes that can be utilized in conjunction with MC. These rely on the idea of Euler discretization and have been worked out extensively in Benth and Benth [2012].

Let time run on a uniform grid of step size Δ, that is $t = 0, \Delta, 2\Delta, ...$ From Kloeden and Platen [1992], Benth and Benth [2012] finds an Euler approximation of SDE 2 given by the p-dimensional time series $\mathbf{x}(t) = (x_1(t), ..., x_p(t))'$ solving the difference equation:

$$\mathbf{x}(t+\Delta) - \mathbf{x}(t) = A\mathbf{x}(t)\Delta + \mathbf{e}_p\sigma(t)\Delta\mathcal{B}(t), \tag{6}$$

where $\Delta\mathcal{B}(t) = \mathcal{B}(t+\Delta) - \mathcal{B}(t)$. We note that in distribution, $\Delta\mathcal{B}(t) = \sqrt{\Delta}\varepsilon(t)$, with $\{\varepsilon(t)\}_{t=0,\Delta,2\Delta,...}$ being standard normal *i.i.d.* This results in a simple recursive schema for simulating $\mathbf{X}(t)$ at discrete times t.

It is possible to increase the simulation accuracy by taking into account the analytical expression for $\mathbf{X}(t)$ as given in Equation 4:

$$\mathbf{X}(t+\Delta) = \exp(A\Delta)\mathbf{X}(t) + \int_t^{t+\Delta} \exp(A(t+\Delta-u))\mathbf{e}_p\sigma(u)d\mathcal{B}(u), \tag{7}$$

The stochastic integral of the equation becomes a p-dimensional Gaussian random variable at each time step t. More specifically, we can define $\mathbf{z}(t)$ as:

$$\mathbf{z}(t) = \int_t^{t+\Delta} \exp(A(t+\Delta-u))\mathbf{e}_p\sigma(u)d\mathcal{B}(u), \tag{8}$$

where $\mathbf{z}(t) \sim N(0, \Sigma_t^z)$. The variance-covariance matrix, Σ_t^z, is given by:

$$\begin{aligned}\Sigma_t^z = cov(\mathbf{z}(t)) &= \int_t^{t+\Delta} \sigma^2(u)\big[\exp(A(t+\Delta-u))\mathbf{e}_p\mathbf{e}_p'\exp(A'(t+\Delta-u))\big]du \\ &= \int_0^{\Delta} \sigma^2(t+\Delta-v)\big[\exp(Av)\mathbf{e}_p\mathbf{e}_p'\exp(A'v)\big]dv.\end{aligned}$$

Additionally, by the increment property of Brownian motion, $\{z(t)\}_{t=0,\Delta,2\Delta,...}$, are independent random variables. Consolidating these results, yields the following simulation scheme for $\mathbf{X}(t)$ given by the discrete time series $\mathbf{x}(t)$:

$$\mathbf{x}(t+\Delta) = \exp(A\Delta)\mathbf{x}(t) + \mathbf{z}(t). \tag{9}$$

As the reader may have noticed, the variance-covariance matrix of $\mathbf{z}(t)$ is time-dependent, leading to inefficient and time-consuming simulations. Benth and Benth [2012] suggests approximating the stochastic integral in Equation 8 by:

$$\int_t^{t+\Delta} \exp(A(t+\Delta-u))\mathbf{e}_p\sigma(u)d\mathcal{B}(u) \approx \exp(A\Delta)\mathbf{e}_p\sigma(t)\Delta\mathcal{B}(t). \tag{10}$$

Additionally, they rewrite the simulation in Equation 9 to the following Euler scheme:

$$\mathbf{x}(t+\Delta) = e^{A\Delta}\mathbf{x}(t) + (\Sigma_t^z)^{1/2}\varepsilon(t), \tag{11}$$

where $\varepsilon(t)$ is a vector of p independent standard normally distributed random walks. Combining the two results, provides an approximative Euler scheme of $\mathbf{X}(t)$ given recursively as the time series:

$$\mathbf{x}(t+\Delta) = \exp(A\Delta)\big[\mathbf{x}(t) + \mathbf{e}_p\sigma(t)\sqrt{\Delta}\varepsilon(t)\big]. \tag{12}$$

4.1.3 Linking ARMA to CARMA

This section identifies the relations that link the CARMA model to the discrete-time ARMA. This will enable us to identify the parameters of a CARMA process, from the estimates obtained from an ARMA process.

We focus on the CAR models only, that is, on the process $Y(t) = X_1(t)$ (where $q = 0$). The derivations and relations which yield a link between continuous-time $AR(p)$ and the discrete-time counterpart in Benth and Benth [2012] result in the following equality:

$$\begin{aligned}
&\frac{1}{\Delta^{p-1}}\sum_{k=0}^{p}(-1)^k b_k^p x_1(t+(p-k)\Delta) \\
&\quad = -\sum_{i=1}^{p} a_{p-i+1}\frac{1}{\Delta^{i-2}}\sum_{k=0}^{i-2}(-1)^k b_k^{i-1}x_1(t+(i-1-k)\Delta) + \\
&\quad\quad + \sigma(t)\sqrt{\Delta}\varepsilon(t),
\end{aligned} \tag{13}$$

where the coefficients b_k^i are defined as $b_0^i = b_i^i = 1$ for $i = 0, ..., p$. Using an $AR(p)$ time series model for $x_1(t)$, we can estimate the coefficients and use equality 13 to find the corresponding parameters $a_1, ..., a_p$ in the CAR(p) dynamics.

We will consider the trivial case of an Ornstein-Uhlenbeck process to verify and provide the reader with some intuition. Consider $p = 1$, such that:

$$\begin{aligned}
b_0^1 x_1(t+\Delta) - b_1^1 x_1(t) &= -a_1\frac{1}{\Delta^{-1}}b_0^0 x_1(t) + \sigma(t)\sqrt{\Delta}\varepsilon(t) \\
\iff x_1(t+\Delta) - x_1(t) &= a_1 x_1(t)\Delta + \sigma(t)\sqrt{\Delta}\varepsilon(t)
\end{aligned} \tag{14}$$

We observe that to estimate the Ornstein-Uhlenbeck process; we can use the first auto regressive coefficient of the $AR(1)$ process. When $p > 1$, we will need to solve a system of equations; this is discussed in more detail in succeeding sections.

4.2 Temperature Dynamics

From multiple empirical analyses in the literature, an AR process with a seasonal component is found to be a suitable model for temperature data. In the following section, we will discuss the motivation of the model and formulate the continuous-time framework.

We will assume that temperature $T(t)$ at time $t \geq 0$ follows CARMA(p,q) dynamics for $q < p$, such that:

$$T(t) = \Lambda(t) + Y(t), \tag{15}$$

where $\Lambda(t)$ a seasonality function and $Y(t) = b'\mathbf{x}(t)$. As long as the matrix A satisfies the conditions for stationarity, and volatility is periodic, we observe that the deseasonalized temperatures are stationary.

In other words, the CARMA(p,q) implies temperature mean-reverts to the seasonal level $\Lambda(t)$. In their empiric research, Benth and Benth [2012] argued for an AR(3) structure for different weather stations in Lithuania. Additionally, they chose a seasonal component defined as:

$$\Lambda(t) = a_0 + a_1 t + a_2 \cos \frac{2\pi t}{365} + a_3 \sin \frac{2\pi t}{365}. \tag{16}$$

During the literature review, we found multiple seasonality functions. For instance, Cabrera [2010] used a truncated Fourier series defined as:

$$\Lambda(t) = a_0 + a_1 t + \sum_{l=1}^{L} a_{l+1} \cos \{ \frac{2\pi(t - d_l)}{l \cdot 365} \}. \tag{17}$$

where the average temperature and global warming are indicated (in both seasonality functions) by the coefficients a_0 and a_1 respectively.

Due to the inherent variability in weather, particularly during winter, the residuals or Y_t, still exhibit a time-varying variance. Following the approach used by Benth and Benth [2012], we utilize a truncated Fourier Series to capture the seasonal patterns evident in the time-varying variance of weather data:

$$f(t) = a_0 + \sum_{n=1}^{N} (a_n \cos(\frac{nt}{365}) + b_n \sin(\frac{nt}{365})), \tag{18}$$

where N is the number of harmonics used in the approximation, a_0 the average value of the function, a_n and b_n respectively the cosine and sine coefficients.

4.3 Pricing Forwards

In this section, different methodologies for pricing weather contracts based on temperature and wind speed are presented and discussed. Consider a forward contract at time t, the arbitrage-free price of the forward contract will be:

$$g(t, \mathcal{T}) = S(t) \exp(r(\mathcal{T} - t)), \tag{19}$$

where r is a constant compounding interest rate, $\mathcal{T}$ the delivery date of the forward, and $S(t)$ is the current spot price. From the general arbitrage pricing theory, we know that a market is free of arbitrage as long as there exists at least one equivalent martingale measure $\mathcal{Q}$.

To derive the explicit price, a specification is needed for the risk-neutral probability measure $\mathcal{Q}$. However, the weather derivatives market is an incomplete market, as weather parameters themselves cannot be stored or traded. Because of this incompleteness, any probability measure Q is equivalent to the real measure P in a risk-neutral measure, yielding a *zero risk premium*.

4.3.1 Temperature Derivatives

Temperature futures are contracts based on a deviation of daily average temperature from a specified reference temperature and measured over specified periods $[\tau_1, \tau_2]$ like weeks, months or quarters of a year. For temperature, the Heating Degree Days (HDD), Cooling Degree Day (CDD), and Cumulative

Averages (CAT) are the most common contracts. These can be mathematically defined as:

$$\text{HDD}(\tau_1, \tau_2) = \int_{\tau_1}^{\tau_2} \max(c - T_u, 0) du, \tag{20}$$

$$\text{CDD}(\tau_1, \tau_2) = \int_{\tau_1}^{\tau_2} \max(T_u - c, 0) du, \tag{21}$$

$$\text{CAT}(\tau_1, \tau_2) = \int_{\tau_1}^{\tau_2} T_u du, \tag{22}$$

where c is a baseline temperature, which is usually $18°C$ or $65°F$, and $T_u = \frac{T_{u,\max} + T_{u,\min}}{2}$ is the average daily temperature on day u. The CDD index is intended to measure the demand for air-conditioning, whereas the HDD measures the demand for heating. The typical seasons of these contracts correspond to when heating demands or cooling demands are high, thus the HDD index usually measures the temperature from October to April whereas the CDD index measures the temperature from April to October. The CAT index substitutes the CDD index for the European cities traded on the CME. A HDD-CDD parity can be deducted from the previous expressions which can be expressed as:

$$\text{CDD}(\tau_1, \tau_2) - \text{HDD}(\tau_1, \tau_2) = \text{CAT}(\tau_1, \tau_2) - c(\tau_2 - \tau_1). \tag{23}$$

As discussed in Section 2.3.1, we will multiply the value of the CDD, HDD or CAT index with the index points ($20) to obtain an actual value of the contract. Additionally, to simplify the portfolio construction, we will create a new contract that implements both the CAT and HDD contract depending on the period within the year. For the winter period (month 10 through 12 and 1 through 4), we will use the HDD value for this contract and for the summer period (month 5 through 9) we will use the value of the CAT index. We will call this new contract the OT contract (Overall Temperature), or mathematically $OT(\tau_1, \tau_2)$, to avoid confusion.

4.4 Portfolio Construction

We define the power output of an asset i as $\xi_{t,i}$ and the selling price of electricity of the asset as P_t^k, for $k = 1, 2, .., 8$. We can then compute the revenue within a given time period (τ_1, τ_2) using:

$$\pi_{t,i}^k(\tau_1, \tau_2) = \sum_{t=\tau_1}^{\tau_2} P_t^k \cdot \xi_{t,i}. \tag{24}$$

The revenues are structured like payoffs. To construct a portfolio with an energy asset's payoff and the different temperature and wind derivatives, we will need to transform the prices of the weather derivative into a payoff as well. For this, we are going to assume that we can only purchase or sell the derivative at the beginning of the month and hold it throughout the month whilst having a daily settlement. This entails that on the first day we have a zero payoff. On each subsequent day, the payoff of the HDD will be positive (negative) if the observed temperature exhibits a more pronounced negative (positive) deviation relative to the mean temperature on that day. For the CDD and CAT indices, the effect on price will be positive (negative) if the deviation from the mean is positive (negative). This is as simple as computing the differential in prices for each day following the initial day within the month.

The payoff of the portfolio can then be constructed as follows:

$$\pi_{t,i}^{k}(\tau_1, \tau_2) + \sum_{j=1}^{L} \gamma_j W_{t,j}(\tau_1, \tau_2), \tag{25}$$

where $W_{t,j}$ the payoff of a certain weather derivative at time t, e.g. the $OT(\tau_1, \tau_2)$ for Amsterdam or Copenhagen. The weight of the payoff of weather derivative j is given by γ_j. As the weather derivatives are monthly strip contracts, we will compute the weights in Equation 25 for every month in a year resulting in 12 different weight vectors for each asset.

The focus is on optimizing the variance-covariance matrix of the payoffs. Because the payoff in Equation 25 can be utilized with multiple weather derivatives, when $L > 1$, we opt not to use the analytical solution to the global minimum variance portfolio. Instead, we follow a different approach. This approach minimizes the variance of Equation 25 each month for each generation type, using the full sample of observations in a given month. For illustration purposes, we optimize the weights for the combination of e.g. January 2020 and fossil gas generation by collecting all observations in January between 2018 and 2023. While this indeed means, that our study has some look-ahead bias, this study is exploratory in the sense of investigating the usefulness of weather derivatives in the context of hedging energy assets.

4.5 Scoring evaluations

There are 4 scoring evaluations chosen. Given that we can express the revenues of the hedged (H) and unhedged (P) portfolios as such:

$$\sum R_{\mathrm{H}} = \pi_{t,i}^{k}(\tau_1, \tau_2) + \sum_{j=1}^{L} \hat{\gamma}_j W_{t,j}(\tau_1, \tau_2), \tag{26}$$

$$\sum R_{\mathrm{P}} = \pi_{t,i}^{k}(\tau_1, \tau_2), \tag{27}$$

the scoring metrics can be defined. Firstly, we define the cost of hedging as a percentage of the regular revenue ($\frac{\sum R_{\mathrm{H}} - R_{\mathrm{P}}}{\sum R_{\mathrm{P}}}$), the variance reduction ($1 - \frac{\sigma^2_{R_{\mathrm{H}}}}{\sigma^2_{R_{\mathrm{P}}}}$), and to obtain a risk-adjusted metric, we show the mean revenue divided by the standard deviation for both the hedged ($\frac{\bar{R_{\mathrm{H}}}}{\sigma_{R_{\mathrm{H}}}}$) and non-hedged portfolio ($\frac{\bar{R_{\mathrm{P}}}}{\sigma_{R_{\mathrm{P}}}}$).

5 Results

In this section, the results of the models imitating the temperature dynamics are shown, additionally, the resulting weather indices are described. This section also describes the portfolios that are consequently built with the weather indices and the energy assets.

The weather data used for the calibration of the CARMA models is from 2000-2018, from this, we simulate 250 series of temperature observations between 2018 and 2023 for each city.

The data used for optimizing the energy portfolios is from 2018-2023. This consists of the electricity generation for each generation type, and the day-ahead prices for each country.

5.1 Temperature Dynamics

The imitation of temperature dynamics is a combination of three kinds of models: a seasonal component (Equation 17), an autoregressive component, and a time-varying variance function (Equation 17). The fitted parameters for the seasonal and autoregressive components can be found in the following table.

		Seasonal Component						Autoregressive Component		
		a_0	$a_1(10^{-3})$	a_2	a_3	d_1	d_2	L1	L2	L3
country	city									
DK	Copenhagen	8.346	0.137	8.353	0.210	-158.138	-73.294	0.907	-0.200	0.096
	Aarhus	8.531	0.115	8.055	0.221	-157.284	-68.305	0.876	-0.150	0.096
FR	Paris	11.352	0.125	7.865	-0.043	-160.843	-1256.779	0.952	-0.248	0.088
	Marseille	15.312	0.141	9.121	0.030	-160.399	38.090	0.862	-0.106	0.048
NL	Amsterdam	10.295	0.099	7.225	0.229	-157.935	-103.658	0.943	-0.227	0.087
	Rotterdam	10.409	0.101	7.343	0.220	-159.275	-108.739	0.946	-0.235	0.087
AT	Vienna	10.335	0.167	10.555	0.071	-165.997	76.849	0.981	-0.248	0.068
	Graz	8.943	0.154	10.082	0.082	-165.942	-522.271	0.934	-0.156	0.036
ES	Madrid	13.877	0.170	10.226	-0.179	-161.093	-46.745	1.003	-0.234	0.054
	Barcelona	16.262	0.128	7.629	-0.102	-154.653	-97.480	0.852	-0.076	0.032
PT	Lisbon	16.564	0.096	5.822	-0.096	-153.380	1.449	0.951	-0.240	0.066
	Porto	15.018	0.092	6.162	-0.110	-154.425	6.416	0.976	-0.243	0.056
IT	Rome	15.350	0.124	8.932	-0.137	-156.428	-122.136	0.905	-0.147	0.051
	Milan	12.626	0.126	10.448	-0.248	-165.227	-96.926	0.929	-0.076	-0.019
BE	Brussels	10.602	0.114	7.569	0.150	-160.536	-93.842	0.954	-0.243	0.083
	Antwerp	10.650	0.109	7.578	0.168	-160.716	-96.579	0.954	-0.240	0.083
DE	Berlin	9.525	0.155	9.698	0.245	-163.559	-48.535	0.973	-0.258	0.096
	Hamburg	9.423	0.128	8.516	0.243	-161.227	-59.963	0.940	-0.224	0.088

Table 4: Fitted parameters of the linear trend, seasonal component, and the AR(3) process on the temperature dynamics.

The coefficient a_0 represents the average temperature value over the dataset. Consequently, we see a higher coefficient in Spain when compared to Denmark due to the warmer climate. The coefficient a_1 captures the linear trend over time. This coefficient, albeit small (notice the 10^{-3}), is positive over the entire range of locations; consistent with our knowledge about climate change. The cosine terms capture the cyclical patterns, with the magnitude of a_{l+1} determining how influential the pattern is. The cyclical patterns are defined on 365 days, or annually, (a_2), and 182.5 days, or semi-annually, (a_3). For visual interpretation, we direct the reader to Figure 8, which visualizes the seasonality component for the different cities.

The coefficients d_{l+1} dictate the phase shift of the cosine wave. From the table, we can see similar impacts of the annual cyclical pattern and a phase shift. The observant reader might notice d_1 to be close to -160 for all cities, this is no coincidence as this aligns with approximately mid-May, the inflection point leading to Summer ($\frac{160}{365} \approx 44\%$ of 12 months). The entire phase shift positions the start of the pattern at around begin-July, ensuring that the wave's peaks and troughs align with the Summer and Winter seasons. When considering the autoregressive components, we find similar coefficients across the locations. However, considering the slight coefficient differences in locations, it makes the most sense to uniquely model all cities independently instead of a generalized model for all.

The fitted parameters for the time-varying variance function can be found in the following table.

		Variance Function								
		a_0	a_1	a_2	a_3	a_4	b_1	b_2	b_3	b_4
country	city									
DK	Copenhagen	3.089	0.853	0.327	0.244	0.121	0.183	-0.265	-0.042	0.008
	Aarhus	2.502	0.722	0.275	0.011	0.096	0.243	-0.133	-0.076	-0.063
FR	Paris	3.488	0.538	0.300	0.000	0.125	0.167	-0.055	0.015	-0.031
	Marseille	2.222	0.649	0.262	0.030	0.042	0.056	-0.136	-0.040	-0.032
NL	Amsterdam	2.757	0.309	0.457	0.099	0.021	0.288	-0.357	-0.042	-0.033
	Rotterdam	3.104	0.393	0.440	0.140	0.051	0.330	-0.344	-0.070	0.003
AT	Vienna	3.888	0.441	0.235	0.024	0.150	0.400	0.158	-0.059	0.049
	Graz	3.152	0.473	0.130	-0.036	0.169	0.298	0.125	0.260	0.124
ES	Madrid	2.478	0.107	-0.001	-0.021	-0.114	0.344	-0.210	0.009	-0.013
	Barcelona	1.457	0.559	-0.037	-0.057	-0.073	0.105	-0.010	0.039	0.035
PT	Lisbon	1.629	-0.084	0.199	0.050	0.020	0.034	-0.015	-0.012	-0.040
	Porto	2.043	-0.268	0.256	0.009	-0.041	-0.026	0.016	-0.061	-0.017
IT	Rome	1.793	0.778	0.203	0.064	-0.050	0.208	-0.071	-0.060	-0.073
	Milan	1.856	-0.011	0.027	-0.062	-0.068	0.243	0.128	-0.052	-0.069
BE	Brussels	3.467	0.375	0.342	0.074	0.082	0.259	-0.113	-0.029	-0.026
	Antwerp	3.302	0.343	0.417	0.099	0.060	0.272	-0.206	-0.017	-0.004
DE	Berlin	3.873	0.306	0.547	0.259	0.135	0.443	-0.148	0.120	0.173
	Hamburg	3.592	0.249	0.506	0.088	0.073	0.475	-0.275	-0.025	-0.015

Table 5: Fitted parameters of truncated Fourier series on the temperature dynamics.

This component is designed to capture the periodic patterns, just like the seasonal and autoregressive component, but it uses both cosine and sine functions. Using both cosine and sine functions allows this component to capture phase shifts more flexibly. Again, for better visual representation, we direct the reader to Figure 8.

Firstly, the seasonality component (in orange) imitates high temperatures in the Summer and low temperatures in the Winter. Secondly, the autoregressive component ensures persistence in the simulated temperatures (in gray). Finally, the variance function (in green) ensures that the variability in temperature, peaking in Winter, is captured in the simulated temperatures as well.

The bottom graphs additionally display the residuals of the fitted components, which somewhat suggest the white noise characteristics of the residuals. Notably, when accounting for the time-varying variance, there's a significant reduction in the absolute value of the residuals. Additional information regarding the residuals can be found in Figure 9.

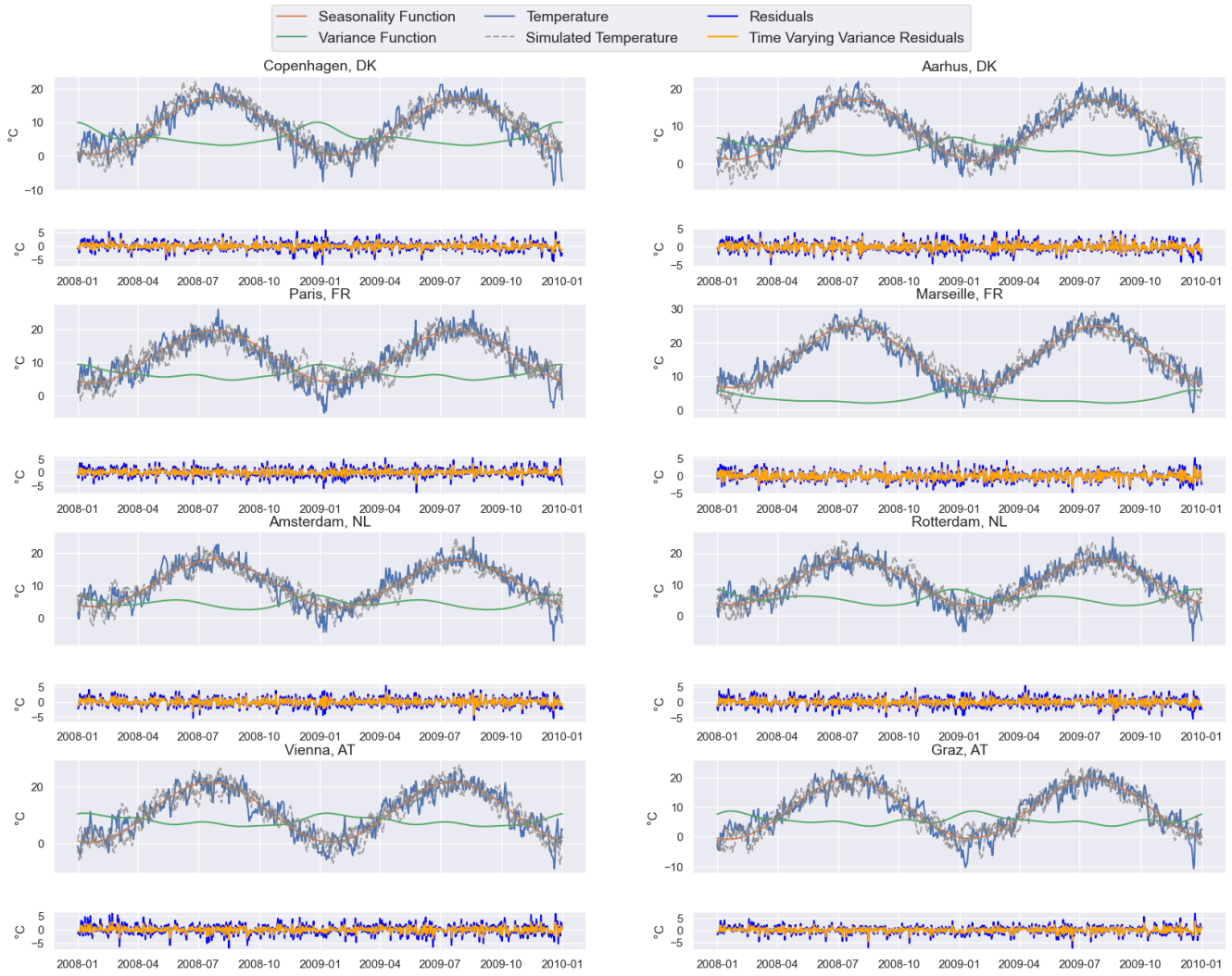

Figure 8: Temperature dynamics between 2008 and 2010 obtained from ECMWF for the described locations. The seasonal component and variance function are formats of truncated Fourier series. The seasonality function is expressed as $\Lambda_t = a_0 + a_1 t + \sum_{l=1}^{2} a_{l+1} \cos\{\frac{2\pi(t-d_l)}{l \cdot 365}\}$. The variance function is expressed as $f(t) = a_0 + \sum_{n=1}^{4}(a_n \cos(\frac{nt}{365}) + b_n \sin(\frac{nt}{365}))$.

While inspecting Figure 9, the residuals of the fitted model indicate that the constructed model is a good fit for modeling the temperature dynamics. Especially when considering the additional component of a time-varying variance (in green), the residuals seem to behave like they are normally distributed. These residuals, for all cities, have zero mean, one standard deviation, their kurtosis near three, and mostly small positive skews. In addition to this, the autocorrelation of the residuals seem to be non-existent. However, when using more stricter tests, like the Jarque-Bera and Kolmogorov-Smirnov tests, we reject the hypothesis of normality.

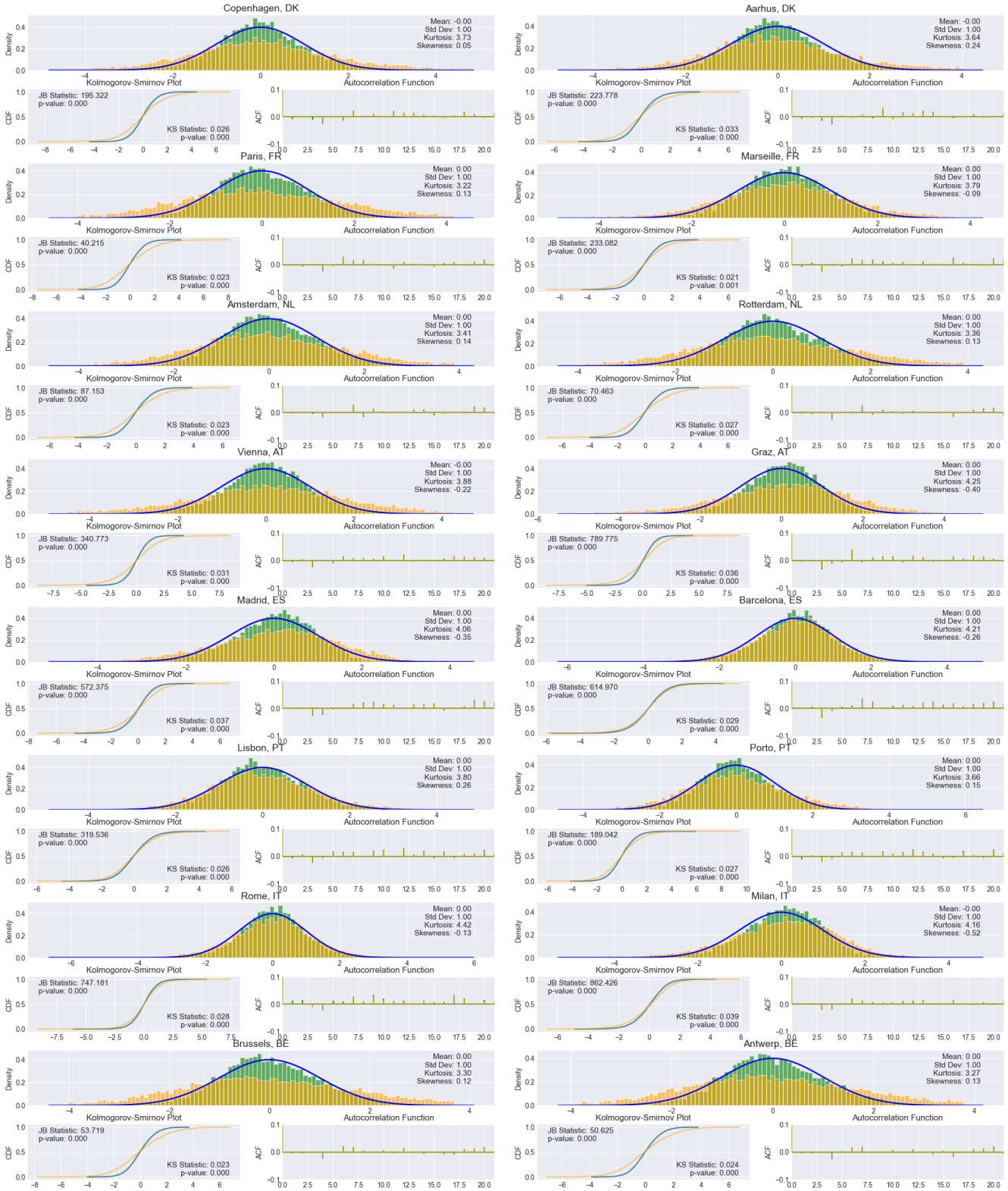

Figure 9: Temperature residuals of the full data spanning 2000 until 2023 obtained from ECMWF using the proposed seasonal component and variance functions. The orange color depicts the residuals on temperature using only the seasonal component, and the green color depicts the residuals using both the seasonal and time-varying variance components. The blue color depicts the normal distribution. The statistics are given for solely the residuals of the combination of the seasonal and time-varying components.

5.2 Weather Derivatives

Using the components mentioned above, we simulate 250 series of temperature observations between 2018-01-01 and 2023-06-01 for each city. These simulations are used to accurately price the temperature indices, as defined in Section 4, using the data known at t. For simplicity, we will purchase or sell a weather derivative at the start of every month and retain this position for the entire month. Additionally, to simplify portfolio construction, we are only holding the HDD and CAT contracts in certain time periods. During the winter months, from October to April, we'll exclusively hold the HDD contract. Conversely, in the summer months, from May to September, we'll maintain the CAT contract. We call this contract OT. Mathematically, this contract at time t is defined as:

$$\mathrm{OT}(t, \tau_1, \tau_2) = \frac{\sum_{i=\tau_1}^{t} \mathrm{OT}(i, \tau_1, \tau_2) + \sum_{j=t+1}^{\tau_2} \widehat{\mathrm{OT}}(j, \tau_1, \tau_2)}{\tau_2 - \tau_1}, \tag{28}$$

where τ_1 and τ_2 respectively reflect the start and end of a single month, and the unknown observations are replaced by the average of the simulated observations $\widehat{\mathrm{OT}}(j, \tau_1, \tau_2)$ at time step j. Using above, we can create a continuous time series of temperature indices. Figure 10 provides a visual interpretation on how the temperature derivatives evolve over time and their reaction to unexpected temperature shocks.

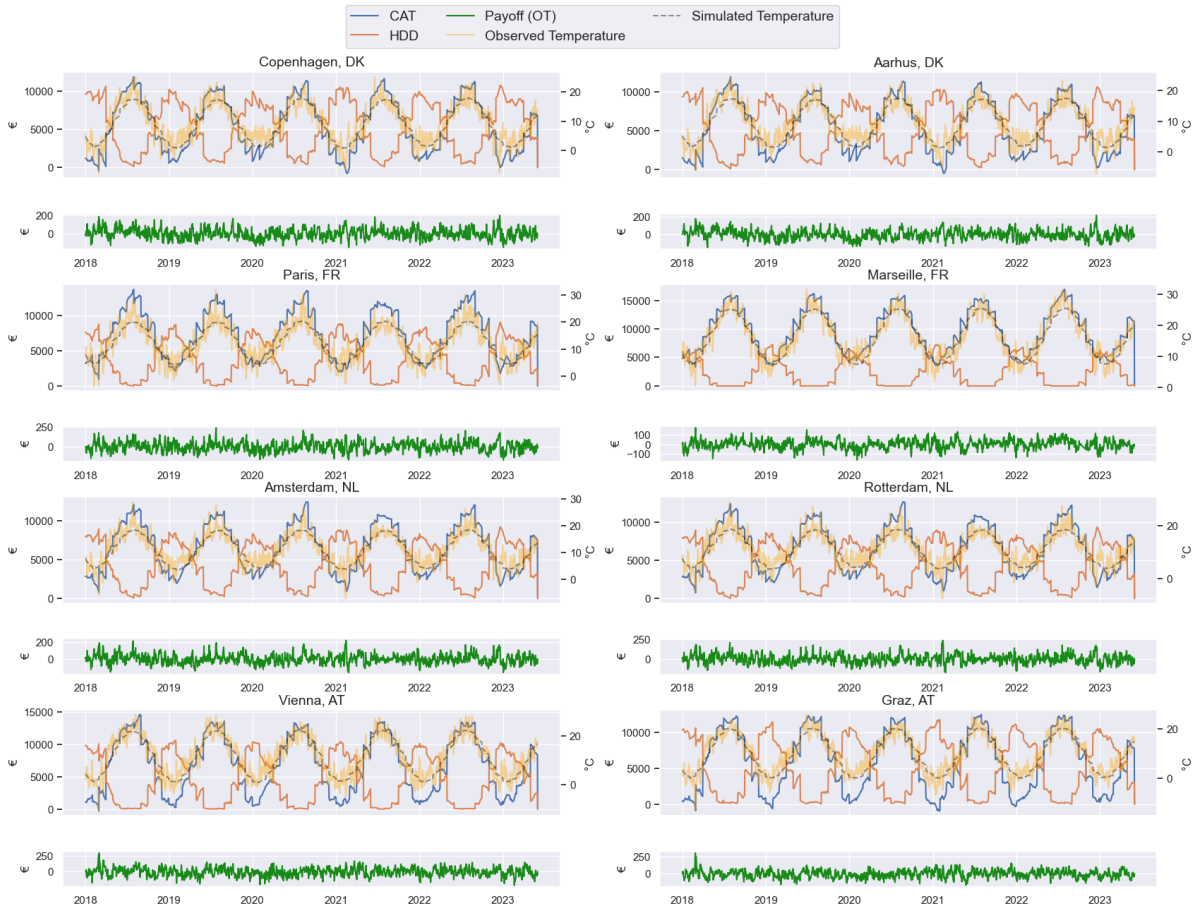

Figure 10: Temperature indices between 2018-01-01 and 2023-06-01, computed using weather data from ECMWF for the described locations.

The CAT index (blue) follows the observed temperature (yellow) the closest, deductible from its definition, the Cumulative Average Temperature index. The HDD index (orange) is almost a mirror image of the CAT index, however responds more moderate in summer periods and more extreme in winter periods. This is due to it being constructed as an index to mainly track heating usage, whereas the CAT index is not particularly seasonally dependent.

The payoffs of the OT derivative, as detailed in Table 6 and partially illustrated in Figure 11, suggest that the payoffs don't strictly follow a normal distribution. The test statistics of the Jarque-Bera test for normality, as well as the Kolmogorov-Smirnov test, confirm this.

Due to the payoffs being a product of temperature, and particularly the (unexpected) temperature deviation, the auto correlation, expressed in days, that's visible in the payoffs makes sense. There is high persistence in temperature, as seen in the preliminary analysis. When temperatures are higher than average, and thus the payoff of the CAT derivative is positive, the temperature (due to the persistence) stays higher than average for a few days, which in turn leads to positive payoffs for a few days. The reverse happens in the winter for the HDD derivative. This persistence is translated back into our OT derivative. Note, that this non-normality can provide problems when constructing portfolios due to the normality assumption.

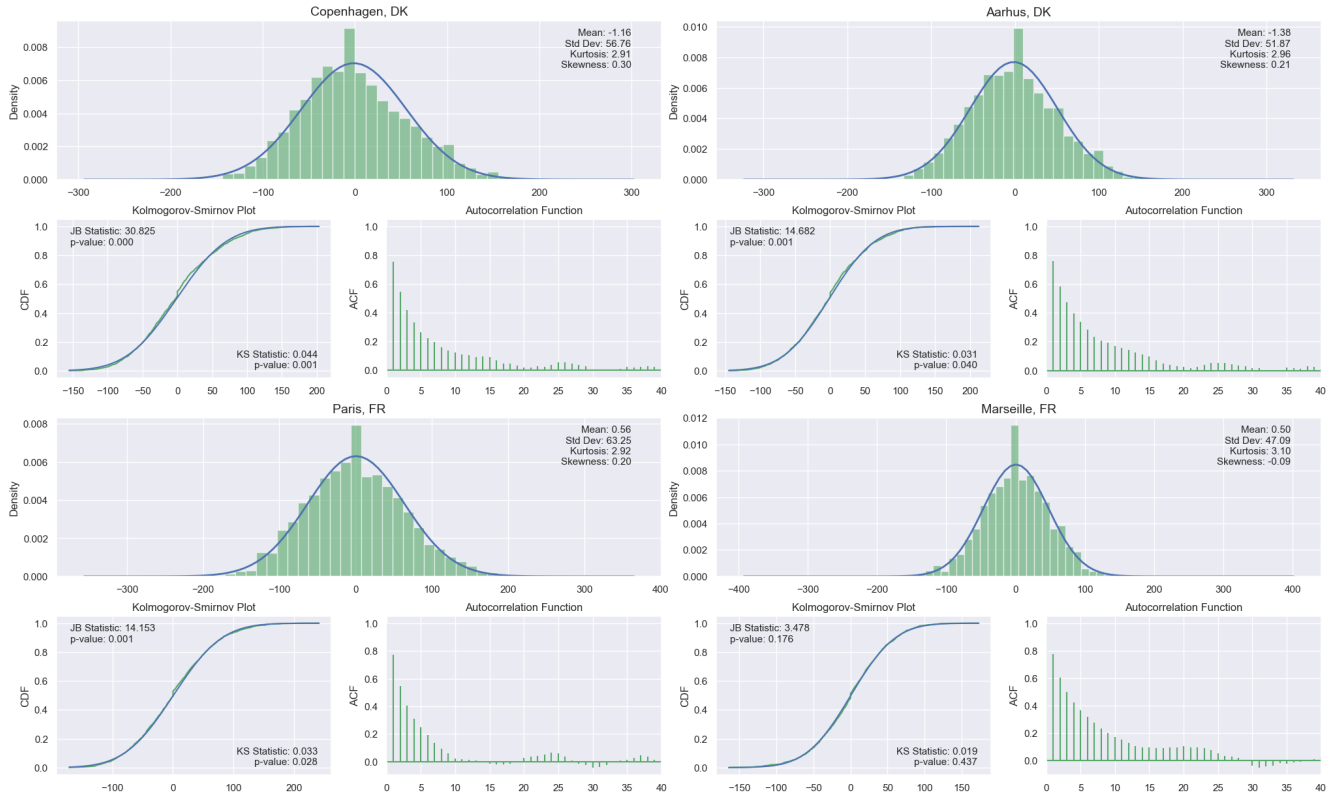

Figure 11: Payoffs for holding the OT derivative for the period of a month. The time period considered is 2008-01-01 and 2023-06-01. The OT derivative is defined as the CAT index in the summer period and the HDD index in the winter period.

Table 6 shows that only except for Spain and France, the daily payoff for holding the OT derivative for the period of a month is negative on average. The average payoff in Austria is quite more negative than in the other countries. The standard deviation is in the same order of magnitude for most cities.

		μ	σ	K	S	KS	KS_p	JB	JB_p
country	city								
DK	Copenhagen	-1.16	56.76	2.91	0.30	0.04	0.00	30.83	0.00
	Aarhus	-1.38	51.87	2.96	0.21	0.03	0.04	14.68	0.00
FR	Paris	0.56	63.25	2.92	0.20	0.03	0.03	14.15	0.00
	Marseille	0.50	47.09	3.10	-0.09	0.02	0.44	3.48	0.18
NL	Amsterdam	-0.97	56.16	3.56	0.46	0.05	0.00	95.90	0.00
	Rotterdam	-1.05	58.84	3.46	0.39	0.04	0.00	66.38	0.00
AT	Vienna	-4.28	64.67	3.12	0.11	0.02	0.30	4.92	0.09
	Graz	-4.53	56.50	3.61	0.16	0.02	0.21	38.46	0.00
ES	Madrid	1.61	58.77	2.68	-0.02	0.03	0.12	8.60	0.01
	Barcelona	1.60	40.13	3.37	-0.11	0.03	0.03	15.20	0.00
NO	Oslo	-0.93	65.57	3.43	0.39	0.06	0.00	64.91	0.00
	Bergen	-1.82	60.81	4.22	0.59	0.05	0.00	237.52	0.00
CH	Zürich	-1.15	61.58	2.74	0.12	0.03	0.03	10.57	0.01
	Geneva	-1.90	61.67	2.60	0.09	0.02	0.21	15.67	0.00
BE	Brussels	-0.65	62.81	3.03	0.21	0.03	0.10	15.20	0.00
	Antwerp	-1.02	61.50	3.17	0.26	0.03	0.06	24.30	0.00
DE	Berlin	-0.15	66.95	3.13	0.26	0.03	0.09	24.27	0.00
	Hamburg	-1.04	63.30	3.00	0.24	0.04	0.00	18.98	0.00

Table 6: Statistics for the payoffs for holding the OT derivative for the period of a month. The KS statistic represents the Kolmogorov-Smirnov test for normality, while the JB statistic represents the Jarque-Bera test for normality.

5.3 Portfolio Construction

This section will discuss and evaluate the portfolios created from a combination of the energy assets, and the weather derivatives.

We will discuss all the generation types in each country, more specifically we discuss fossil gas, fossil hard coal, nuclear, solar, wind offshore, and wind onshore. We do this by using the entire generation from a certain type of generation (e.g. wind, or fossil gas), and multiplying this by the day-ahead price at the time of generation. This results in proxy revenue of the entire generation group, which will be hedged by a temperature index. For simplicity, we use the temperature index of the capital of each country. The weights for the minimum variance portfolio are computed for each month. The results are completely in-sample, as all the data is used to compute the weights, see also Portfolio Construction in Section 4.

There are 4 scoring evaluations chosen, which correspond to the cost of hedging as a percentage of the regular revenue ($\frac{\sum R_{\mathrm{H}} - R_{\mathrm{P}}}{\sum R_{\mathrm{P}}}$), the variance reduction ($1 - \frac{\sigma^2_{R_{\mathrm{H}}}}{\sigma^2_{R_{\mathrm{P}}}}$), and to obtain a risk-adjusted metric, we show the mean revenue divided by the standard deviation for both the hedged ($\frac{\bar{R_{\mathrm{H}}}}{\sigma_{R_{\mathrm{H}}}}$) and non-hedged portfolio ($\frac{\bar{R_{\mathrm{P}}}}{\sigma_{R_{\mathrm{P}}}}$).

Starting in Table 7 [1], describing the portfolios constructed for Fossil Gas, we see positive variance reductions when utilizing temperature indices to minimize variance. When comparing the risk-adjusted metrics, we notice that for all countries except Italy the hedged portfolio has a higher risk-adjusted expected revenue. Additionally, from the table we see that the cost of hedging is negative, for all countries except Austria. For Austria, this means that the hedged portfolio actually yields higher revenues than the unhedged portfolio.

Combining the cost of revenue and variance reduction, we can conclude from the table that for most countries, the variance reduction is a multiple of the cost of hedging. Especially for Denmark and Spain, which are both standing out with a variance reduction of about 15% at a cost of about 2%.

Looking at the weights, we notice a lot of variability across the countries and months. Not only does the climate and average temperature have an impact, but as we are using a two-fold derivative (HDD in winter period and CAT in summer period) the sign of the weight can suddenly switch from positive to negative.

Recall that between May and September the Cumulative Average Temperature (CAT) index is used, that is a positive weight given to the index during this period pays out when the temperature is higher than expected, or hotter summers, whereas a negative weight represents protection against colder summers. Between October and April, the Heating Degree Days (HDD) index is used, that is a positive weight during this period pays out when the temperature is lower than expected, or colder winters, whereas a negative weight represents protection against hotter winters.

Overall, most countries hold a negative weight for the fossil gas portfolio during the winter period, implying protection against hotter winters. Hotter winters mean less power consumption, less demand,

[1] Electricity from these portfolios is traded on day-ahead electricity markets and hedged using a single monthly temperature index (capital of the country). In this table, R_{P} represents the revenue from the generation portfolio, while R_{H} denotes the revenue from the hedged portfolio. The analysis spans from January 1, 2018, to June 1, 2023. The weights are normalized by the average generation over the entire period.

and therefore lower prices and revenue. Additionally, regular gas consumption for heating might play a role in these weights. However, in September most weights seem to be positive except for Portugal and the Netherlands, implying protection against hotter summers.

Fossil Gas	AT	BE	DE	DK	ES	FR	IT	NL	PT
	Scoring evaluation								
$\frac{\sum R_H - R_P}{\sum R_P}$	1.372	-0.799	-0.554	-1.925	-1.979	-0.777	-4.730	-1.215	-1.759
$\frac{R_H}{\sigma_{R_H}}$	0.871	1.033	0.987	1.974	1.713	0.915	0.928	1.081	1.489
$\frac{R_P}{\sigma_{R_P}}$	0.844	1.010	0.968	1.849	1.617	0.897	0.944	1.071	1.442
$1 - \frac{\sigma^2_{R_H}}{\sigma^2_{R_P}}$	3.626	5.889	4.952	15.634	14.399	5.405	6.079	4.202	9.442
	Weights evaluation								
January	-0.027	-0.429	-0.052	-0.228	-0.020	-0.413	-0.399	-0.171	-0.106
February	-0.164	-0.031	0.002	-0.179	0.584	-0.054	-0.056	0.018	0.676
March	-0.447	0.054	-0.041	-0.064	-0.104	0.017	-0.472	0.066	-0.494
April	-0.596	-0.314	-0.335	0.001	0.132	-0.708	-0.742	-0.252	0.187
May	-1.284	-0.232	-0.045	0.133	-0.031	-0.672	-0.245	-0.033	-0.141
June	-1.089	0.187	0.648	-0.035	-0.049	0.063	-1.695	0.363	0.004
July	-0.470	-0.143	-0.062	0.222	-0.150	-0.560	-1.942	-0.053	-0.030
August	-0.425	-0.518	-0.464	0.024	0.075	-0.870	-0.258	-0.430	-0.058
September	0.518	0.046	0.112	0.209	0.037	0.126	0.089	-0.231	-0.021
October	-0.040	0.182	0.170	-0.084	-0.053	0.487	0.172	0.332	-0.082
November	-0.347	-0.210	-0.119	-0.075	-0.050	-0.166	-0.088	-0.035	-0.246
December	-0.386	-0.530	-0.667	-0.150	0.145	-0.549	0.139	-0.559	0.068

Table 7: Characteristics of fossil gas generation portfolios for selected countries utilizing natural gas as an energy source.

Fossil Hard Coal	AT	DE	DK	ES	FR	IT	NL	PT
	Scoring evaluation							
$\frac{\sum R_H - R_P}{\sum R_P}$	-2.391	-0.188	-0.720	-1.702	1.633	-2.974	-0.563	-0.588
$\frac{R_H}{\sigma_{R_H}}$	0.465	0.955	1.844	1.150	0.567	1.027	0.998	1.017
$\frac{R_P}{\sigma_{R_P}}$	0.468	0.938	1.743	1.121	0.525	1.018	0.994	0.987
$1 - \frac{\sigma^2_{R_H}}{\sigma^2_{R_P}}$	3.433	3.868	11.885	8.192	11.396	7.504	1.849	6.890
	Weights evaluation							
January	-0.390	-0.069	-0.154	-0.194	-0.961	-0.092	-0.062	-0.347
February	0.098	0.016	-0.207	-0.141	-0.361	-0.337	0.037	-0.595
March	0.088	-0.144	-0.061	-0.167	-0.298	-0.293	-0.068	0.022
April	0.495	-0.312	0.120	-0.120	-0.581	-0.365	-0.190	-0.391
May	0.366	-0.134	0.164	0.126	-0.194	-0.610	-0.113	0.228
June	-0.660	0.507	0.153	0.027	0.101	-1.719	0.575	-0.077
July	0.088	-0.089	0.128	0.330	-0.453	-2.100	0.106	-0.047
August	-0.895	-0.262	-0.017	-0.687	-0.144	-0.168	-0.273	-0.355
September	-0.162	0.039	0.009	-0.798	-0.390	0.342	-0.301	-0.314
October	0.406	-0.103	-0.143	-0.092	-0.737	0.475	-0.030	0.118
November	0.071	-0.267	0.014	0.209	-1.013	-0.036	-0.169	-0.449
December	-0.105	-0.653	-0.197	-0.328	-1.382	0.381	-0.348	-0.948

Table 8: Characteristics of coal generation portfolios for selected countries utilizing coal as an energy source.

The scoring evaluation in Table 8, representing energy generation using fossil hard coal, looks com-

parable to the previous table. However, the average risk-adjusted revenue is slightly lower overall than for fossil gas. Given that the installed capacity (see Table 1) for fossil hard coal is comparably low for the entirety of Europe, except for Germany, these results are to be expected. The highest variance reductions are achieved in France (11.4%) and Denmark (11.9%), with Spain (8.2%) and Italy (7.5%) following closely.

Moving to the nuclear generation, depicted in Table 9, we again find a high variance reduction for Spain (16.9%). Additionally, we find much higher average risk-adjusted revenues. As a nuclear power plant cannot be simply turned off, nuclear generation is very constant over time, leading to higher average risk-adjusted revenues. However, the difference between the hedged and unhedged portfolios is not as significant as for the other generation types; with the hedged portfolio only performing marginally better.

Nuclear	BE	DE	ES	FR	NL
	Scoring evaluation				
$\frac{\sum R_H - R_P}{\sum R_P}$	-0.505	0.278	-3.809	-0.541	-1.161
$\frac{\bar{R}_H}{\sigma_{R_H}}$	1.098	1.815	1.902	1.313	1.021
$\frac{\bar{R}_P}{\sigma_{R_P}}$	1.098	1.806	1.803	1.311	1.022
$1 - \frac{\sigma^2_{R_H}}{\sigma^2_{R_P}}$	1.053	0.339	16.860	1.445	2.073
	Weights evaluation				
January	-0.007	-0.021	0.011	-0.086	0.141
February	0.072	0.010	0.359	0.059	0.125
March	0.106	-0.000	0.135	0.065	0.118
April	-0.209	-0.100	0.154	-0.216	-0.034
May	-0.163	0.003	0.000	-0.128	-0.063
June	0.123	0.163	-0.010	-0.029	1.066
July	0.103	-0.046	0.034	-0.090	0.075
August	-0.197	0.022	-0.070	-0.200	-0.302
September	-0.011	-0.053	-0.173	0.055	-0.181
October	0.206	-0.010	0.014	0.060	0.313
November	0.034	-0.059	0.047	-0.140	0.127
December	-0.128	-0.057	0.715	-0.173	-0.240

Table 9: Characteristics of nuclear generation portfolios for selected countries utilizing nuclear as an energy source.

The solar generation, as seen in Table 10, show, much like what was seen previously, that the biggest variance reduction can be achieved in Italy, Spain and Portugal. The risk-adjusted returns show only marginal improvement for the other countries. Much like solar, the hydro generation (in Table 11) provides the same conclusion, with the highest variance reductions being found in Southern Europe.

Finally, moving to the portfolios utilizing wind generation, we see that the highest improvements can be achieved in Southern Europe. Still, for both offshore and onshore, variance reductions can be achieved all throughout Europe. However, the average risk-adjusted revenue is only marginally better in the hedged portfolio.

Solar	AT	BE	DE	DK	ES	FR	IT	NL	PT
	Scoring evaluation								
$\frac{\sum R_{\mathrm{H}} - R_{\mathrm{P}}}{\sum R_{\mathrm{P}}}$	0.971	-0.468	0.550	0.372	-1.757	-0.984	-3.759	-1.565	-0.930
$\frac{\bar{R}_{\mathrm{H}}}{\sigma_{R_{\mathrm{H}}}}$	0.718	0.625	0.700	1.031	1.011	0.676	0.820	0.545	0.917
$\frac{\bar{R}_{\mathrm{P}}}{\sigma_{R_{\mathrm{P}}}}$	0.709	0.624	0.696	1.042	0.995	0.674	0.815	0.548	0.889
$1 - \frac{\sigma^2_{R_{\mathrm{H}}}}{\sigma^2_{R_{\mathrm{P}}}}$	0.582	1.153	0.132	-2.817	6.579	2.451	8.499	1.933	7.870
	Weights evaluation								
January	0.376	-0.056	0.322	-0.198	-0.165	-0.259	-0.338	0.180	-0.032
February	0.041	-0.076	0.122	-0.019	0.363	0.076	-0.155	0.123	0.550
March	-0.200	0.152	0.063	0.029	0.341	0.083	-0.357	0.445	0.337
April	-0.373	-0.284	-0.246	0.063	0.606	-0.370	-0.636	-0.493	1.116
May	-0.468	-0.170	-0.037	0.186	-0.059	-0.336	-0.479	-0.072	-0.277
June	-0.089	0.353	0.620	0.212	-0.051	-0.078	-1.672	0.798	-0.043
July	-0.159	0.205	0.117	-0.113	0.076	-0.219	-2.245	0.298	0.020
August	-0.441	-0.393	-0.038	-0.087	0.019	-0.590	0.204	-0.522	0.025
September	0.424	-0.093	0.133	0.182	-0.162	0.323	0.282	-0.676	-0.082
October	-0.019	0.220	0.192	-0.027	0.154	0.174	0.007	0.531	0.107
November	0.038	0.366	0.317	-0.026	-0.047	0.101	-0.329	0.551	-0.182
December	-0.113	-0.605	-0.017	0.109	1.353	-0.316	0.321	-0.801	1.704

Table 10: Characteristics of solar generation portfolios for selected countries utilizing solar as an energy source.

Hydro: Run of River	AT	BE	DE	DK	ES	FR	IT	PT
	Scoring evaluation							
$\frac{\sum R_{\mathrm{H}} - R_{\mathrm{P}}}{\sum R_{\mathrm{P}}}$	1.710	1.392	0.604	0.597	-3.139	0.107	-2.588	-2.556
$\frac{\bar{R}_{\mathrm{H}}}{\sigma_{R_{\mathrm{H}}}}$	1.095	0.928	1.475	2.546	2.256	1.227	1.359	1.041
$\frac{\bar{R}_{\mathrm{P}}}{\sigma_{R_{\mathrm{P}}}}$	1.077	0.905	1.463	2.494	2.157	1.222	1.314	0.952
$1 - \frac{\sigma^2_{R_{\mathrm{H}}}}{\sigma^2_{R_{\mathrm{P}}}}$	-0.023	2.185	0.358	2.868	14.242	0.651	11.211	20.706
	Weights evaluation							
January	0.476	-0.088	0.086	0.033	0.022	-0.039	-0.140	0.116
February	0.068	-0.086	0.014	0.018	0.122	0.042	-0.054	-0.198
March	-0.015	0.013	-0.006	0.167	0.021	0.090	-0.209	-0.415
April	-0.135	-0.099	0.012	0.070	-0.011	-0.194	0.089	-0.161
May	-0.451	-0.073	-0.160	0.123	0.021	-0.199	-0.218	0.185
June	-0.094	0.096	0.271	0.031	0.094	0.001	-0.674	-0.269
July	0.007	0.357	-0.031	-0.039	0.196	0.010	-1.036	-0.008
August	0.049	0.694	-0.029	-0.072	-0.163	-0.141	-0.083	-0.310
September	0.410	-0.061	0.069	0.115	-0.269	0.099	-0.000	-0.125
October	-0.117	-0.195	0.105	0.185	-0.148	0.186	-0.374	-0.086
November	-0.041	-0.236	-0.034	0.041	0.035	0.028	-0.150	-0.026
December	0.084	0.163	-0.087	0.023	0.492	-0.080	0.199	1.309

Table 11: Characteristics of hydro generation portfolios for selected countries utilizing hydro as an energy source.

Wind Offshore	BE	DE	DK	FR	IT	NL	PT
	Scoring evaluation						
$\frac{\sum R_{\mathrm{H}} - R_{\mathrm{P}}}{\sum R_{\mathrm{P}}}$	-1.252	-1.712	-0.405	-0.153	-0.254	-1.731	-13.628
$\frac{\bar{R}_{\mathrm{H}}}{\sigma_{R_{\mathrm{H}}}}$	0.713	0.972	1.109	0.028	0.268	0.729	0.332
$\frac{\bar{R}_{\mathrm{P}}}{\sigma_{R_{\mathrm{P}}}}$	0.712	0.968	1.111	0.028	0.266	0.732	0.344
$1 - \frac{\sigma^2_{R_{\mathrm{H}}}}{\sigma^2_{R_{\mathrm{P}}}}$	2.828	4.038	0.412	0.003	1.373	2.586	20.144
	Weights evaluation						
January	0.554	0.402	0.264	0.145	1.795	0.619	0.322
February	0.198	0.183	-0.046	-0.132	-1.093	0.239	1.303
March	0.166	0.031	-0.070	0.055	1.511	0.127	1.160
April	-0.302	-0.223	0.011	-0.077	-0.494	-0.281	1.391
May	-0.222	-0.109	0.392	0.018	0.990	-0.120	-0.451
June	-0.139	0.445	-0.120	0.086	-8.606	0.518	-1.551
July	-0.146	0.005	0.011	0.099	-4.308	-0.244	-0.632
August	0.117	0.089	-0.154	-0.045	2.954	0.063	0.712
September	0.292	-0.001	0.092	0.033	5.299	0.341	0.875
October	0.406	0.114	0.242	-0.088	4.489	0.500	0.456
November	0.253	0.181	0.243	0.072	-1.780	0.478	0.298
December	0.197	-0.101	-0.055	-0.064	1.797	-0.076	5.322

Table 12: Characteristics of wind offshore generation portfolios for selected countries utilizing wind offshore as an energy source.

Wind Onshore	AT	BE	DE	DK	ES	FR	IT	NL	PT
	Scoring evaluation								
$\frac{\sum R_{\mathrm{H}} - R_{\mathrm{P}}}{\sum R_{\mathrm{P}}}$	-0.008	-2.574	-3.260	-0.721	-3.573	-2.329	-1.368	-2.262	-3.742
$\frac{\bar{R}_{\mathrm{H}}}{\sigma_{R_{\mathrm{H}}}}$	0.808	0.729	0.845	1.189	1.122	0.830	0.765	0.721	1.131
$\frac{\bar{R}_{\mathrm{P}}}{\sigma_{R_{\mathrm{P}}}}$	0.799	0.727	0.841	1.187	1.134	0.833	0.770	0.725	1.074
$1 - \frac{\sigma^2_{R_{\mathrm{H}}}}{\sigma^2_{R_{\mathrm{P}}}}$	2.241	5.468	7.270	1.658	5.059	4.077	1.301	3.459	16.447
	Weights evaluation								
January	0.354	0.785	0.560	0.450	-0.104	0.527	0.009	0.630	0.155
February	0.201	0.215	0.312	-0.075	0.035	0.207	0.147	0.336	0.250
March	-0.222	0.291	0.082	-0.178	0.183	0.328	-0.048	0.202	0.204
April	-0.065	-0.317	-0.268	-0.030	0.034	-0.362	-0.243	-0.277	-0.109
May	-0.276	-0.026	-0.133	0.385	0.042	-0.028	-0.016	-0.168	-0.219
June	0.058	-0.140	0.476	-0.034	0.025	-0.325	-1.021	0.413	0.059
July	0.195	-0.136	0.010	-0.011	-0.020	-0.191	-0.792	-0.037	0.028
August	0.087	-0.119	0.039	-0.020	-0.100	-0.374	0.281	-0.080	0.092
September	0.491	-0.021	0.118	-0.015	-0.055	0.304	0.828	0.098	-0.052
October	-0.260	0.604	0.169	0.237	-0.061	0.644	-1.158	0.572	-0.197
November	-0.174	0.412	0.233	0.178	0.000	0.295	-0.093	0.543	0.115
December	-0.005	0.386	0.189	0.061	0.638	0.198	0.247	0.170	1.474

Table 13: Characteristics of wind onshore generation portfolios for selected countries utilizing wind onshore as an energy source.

6 Conclusion

In this section, the key findings, as well as contributions of this paper, are provided. Additionally, a discussion followed by the limitations and potential further research is provided.

This research extends from Benth et al. [2011] and investigates the potential weather derivatives might offer in hedging energy assets. The weather data is obtained for 18 European cities between 2000 and 2023, electricity generation and price data is obtained for the period 2018 until 2023. The temperature is decomposed into three different components, a seasonal component, an autoregressive component, and a time-varying variance component. Afterwards, 250 temperature simulations are obtained from this decomposition; from which two temperature indices are created, the Cumulative Average Temperature (CAT) index and Heating Degree Days (HDD) index. These indices are transformed into a new derivative, which holds a HDD contract in the winter, and a CAT index in the summer. Using this derivative, portfolios are created for each generation type in the countries, and optimized for minimum variance every month.

The results offer insight in the potential of weather derivatives decreasing the total variance of energy portfolios. From the results, we draw that significant variance reduction can be achieved using a simple buy-and-hold strategy for monthly temperature indices. This is especially true for Southern European countries, like Spain, Italy and Portugal. The cost of hedging, as a percentage of the total revenue, is a fraction of the variance reduction.

The first research question, regarding the effectiveness of the decomposition of temperature, is described in great detail in Benth et al. [2011]. However, this thesis extends this by providing residual statistics for multiple locations. We can conclude, that while the proposed model is effective in its own regard, the residuals are not completely white noise. There is still some kurtosis, autocorrelation, and skewness left in the residuals.

The second research question investigates whether temperature derivatives are effective at hedging a portfolio of energy assets. While in this research, we focussed mainly on complete country generation portfolios, the derivatives certainly reduced total variances in the energy portfolios.

Thirdly, the differences between the energy asset type portfolios, are mainly characterized by the weights of the temperature derivative. Whilst most energy types prefer negative weights over the winter, protecting against hotter winters, wind offshore and onshore actually held positive weights over the winter, therefore protecting against colder winters.

The above findings result in the conclusion that there definitely exist applications of weather derivatives that reduce variances of energy portfolios, which provides more constant revenue streams. In addition to this, it provides the basic fundamentals of pricing weather derivatives, and requesting appropriate data, under an Open-Source license available on the author's Github.

6.1 Limitations and Further Research

This thesis draws upon data from nine countries, encompassing both weather and electricity data. As a result, the scope of the study is broad, leaving limited room for a detailed examination of specific regions, such as the Netherlands. This breadth may have obscured some of the potential benefits of using weather

derivatives as tools for variance reduction.

For more detailed insights, future research should consider narrowing the focus to assets in a specific geographical area. This targeted approach would also facilitate a more in-depth exploration of the impact on various Power Purchase Agreements (PPAs), a topic that remains largely unexplored in the current study.

Furthermore, while the software developed for this thesis is capable of hedging portfolios with multiple temperature derivatives (e.g. CDD Amsterdam and HDD Berlin), its practical application was limited due to the expansive geographical focus. Therefore, it is strongly recommended that subsequent studies focus on a more specific region and asset type.

Finally, as previously discussed, the study has some look-ahead bias due to utilizing the full sample for the estimation of the weights. Therefore, this study is purely exploratory in investigating the usefulness of weather derivatives in the context of hedging energy assets. To truly gauge how effective the hedging can be, the weights need to be estimated and tested against out-of-sample data.

References

P. Alaton, B. Djehiche, and D. Stillberger. On modelling and pricing weather derivatives. *Applied Mathematical Finance*, 9(1):1–20, 2002. doi: 10.1080/13504860210132897. URL https://doi.org/10.1080/13504860210132897.

F. E. Benth and J. Benth. *Modeling and Pricing in Financial Markets for Weather Derivatives*. WORLD SCIENTIFIC, 2012. doi: 10.1142/8457. URL https://www.worldscientific.com/doi/abs/10.1142/8457.

F. E. Benth, J. S. Benth, and V. Kholodnyi. Calibration of temperature futures by changing the mean reversion. *Applied Mathematical Finance*, 18(3):245–263, 2011. doi: 10.1080/13504851.2010.505669.

F. E. Benth, T. S. Christensen, and V. Rohde. Multivariate continuous-time modeling of wind indexes and hedging of wind risk. *Quantitative Finance*, 21:165–183, 2021. doi: 10.1080/14697688.2020.1804606.

P. J. Brockwell. Lévy-driven carma processes. *Annals of the Institute of Statistical Mathematics*, 53(1):113–124, 2001. doi: 10.1023/A:1017972605872.

B. L. Cabrera. *Weather Risk Management: CAT bonds and Weather Derivatives*. PhD thesis, Humboldt-Universität zu Berlin, 2010. URL https://edoc.hu-berlin.de/bitstream/handle/18452/16833/lopez-cabrera.pdf?sequence=1.

CME Group. Weather futures and options. https://www.cmegroup.com/trading/weather/files/weather-fact-card.pdf, 2021. [Online; accessed 24-11-2022].

J. L. Doob. The elementary gaussian processes. *The Annals of Mathematical Statistics*, 15(2):229–282, 1944.

F. Dornier and M. Querel. Caution to the wind. *Energy Power Risk Management: Weather Risk Special Report*, pages 30–32, 2000.

P. H. Franses, J. Neele, and D. van Dijk. Modeling asymmetric volatility in weekly dutch temperature data. *Environmental Modelling & Software*, 16(2):131–137, 2001. ISSN 1364-8152. doi: 10.1016/S1364-8152(00)00076-1. URL https://www.sciencedirect.com/science/article/pii/S1364815200000761.

W. K. Härdle et al. Pricing wind power futures. *Journal of the Royal Statistical Society Series C: Applied Statistics*, 70(4):1083–1102, August 2021. doi: 10.1111/rssc.12499.

P. E. Kloeden and E. Platen. *Numerical Solution of Stochastic Differential Equations*, volume 23 of *Stochastic Modelling and Applied Probability*. Springer, 1992.

R. S. Tol. Autoregressive conditional heteroscedasticity in daily temperature measurements. *Environmetrics*, 7(1):67–75, 1996. doi: https://doi-org.eur.idm.oclc.org/10.1002/(SICI)1099-095X(199601)7:1⟨67::AID-ENV164⟩3.0.CO;2-D. URL https://onlinelibrary-wiley-com.eur.idm.oclc.org/doi/abs/10.1002/%28SICI%291099-095X%28199601%297%3A1%3C67%3A%3AAID-ENV164%3E3.0.CO%3B2-D.

K. Tolstrup, J. Lago, and L. Vries. Effect of market design on strategic bidding behavior: Model-based analysis of european electricity balancing markets. *Applied Energy*, 270:115130, 07 2020. doi: 10.1016/j.apenergy.2020.115130.